GIS-BASED QUANTITATIVE INTEGRATION OF GLOBAL CLIMATE MODEL
SIMULATIONS AND GEODATABASES OF GULLIES ON MARS

by

James Langley Dickson

A Thesis Presented to the
FACULTY OF THE USC GRADUATE SCHOOL
UNIVERSITY OF SOUTHERN CALIFORNIA
In Partial Fulfillment of the
Requirements for the Degree
MASTER OF SCIENCE
(GEOGRAPHIC INFORMATION SCIENCE AND TECHNOLOGY)

June 2014

DEDICATION

For Nancy Struble Dickson, a supporter of science, the space program, and her sons.

ACKNOWLEDGMENTS

The genesis of this project was in 2011, when we learned that Mars had a massive slab of dry ice trapped in its south polar cap, and that when it used to be in the atmosphere, Mars was a different place than it is today. I had ideas about what this could mean for water on Mars, but lacked the skills to test them. I have them now, and it is a result of what I've learned through the USC Spatial Sciences Institute. The efficiency of the program and the diversity of the curriculum are, I hope, reflected in this thesis.

I appreciate the assistance of my committee: Flora Paganelli, Darren Ruddell and Jordan Hastings. Specifically, Flora provided guidance at all scales, from the scope of the project to the clarity of the writing to the justification of paragraphs. Her thoughtfulness and planetary experience were the reasons that I hoped she would be my chair, and the reasons I was happy to find out that she was. Robert Vos and Mariko Dawson Zare were also very helpful at the outset of this thesis, and John Wilson provided a valuable review of this work on very short notice.

My mother, Nancy Dickson, late father, James G. Dickson, and brother, Bob Dickson, provided an environment for me that encouraged inquiry and humility, and were patient as I took my time figuring out what I wanted to be when I grew up. It would have happened sooner, if Mars and Antarctica were not so far away.

Jim Head has allowed me to build the planetary GIS and visualization lab of my dreams, and every number crunched in this thesis was crunched on a workstation in his lab. Besides resources, his patience while I completed this was, I hope, a function of his trust in me when I said that I was creating something that would be of value to his lab.

TABLE OF CONTENTS

LIST OF TABLES

LIST OF FIGURES

LIST OF ABBREVIATIONS

CTX   Context Camera

GCM   Global Climate Model / General Circulation Model

GFDL   Geophysical Fluid Dynamics Laboratory

GIS   Geographic Information Science

HiRISE   High Resolution Imaging Science Experiment

HRSC   High Resolution Stereo Camera

ISIS   Integrated Software for Imagers and Spectrometers

JPL   Jet Propulsion Laboratory

LDM   Latitude Dependent Mantle

LMD   Laboratoire de Météorologie Dynamique

MOC   Mars Orbiter Camera

MRO   Mars Reconnaissance Orbiter

NASA   National Aeronautics and Space Administration

PDS   Planetary Data System

PIGWAD   Planetary Interactive G.I.S.-on-the-Web Analyzable Database

THEMIS   Thermal Emission Imaging System

USGS   United States Geological Survey

ABSTRACT

Global climate models (GCMs) allow planetary scientists to test physical explanations for the formation and modification of climate-related features on planetary bodies. This method of analysis depends upon two data sources: the GCM itself and a catalog of features under investigation. Integrating these two inputs provides a novel approach for testing climate-related hypotheses for the formation of geological features of interest. An integration pipeline has been developed and a proof-of-concept application is tested on martian gullies, small erosional channels that may provide evidence for the recent flow of liquid water on the surface of Mars.

The end-to-end GCM/data integration approach includes three primary components: (1) generation of a geodatabase with coded domains of all imaged gullies in the southern hemisphere of Mars from Mars Reconnaissance Orbiter (MRO) Context Camera (CTX) images, (2) incorporation into a Geographic Information System (GIS) framework of three GCM simulations that quantitatively predict surface conditions over one martian year under three different starting scenarios thought to have occurred in Mars' recent geologic history, and (3) the integration of the geodatabase and GCM simulations to create dynamic visualizations of surface conditions over time and quantitative extraction of temperature/pressure values at gully sites to test whether or not liquid water could exist at these locations.

The newly developed approach in this study demonstrates that the formation of gullies by liquid water is unlikely under present atmospheric conditions at most locations, but is predicted to have been achievable under more favorable orbital scenarios thought to have occurred in the recent geologic history of Mars. If these associations are valid,

this increases the potential of primitive biology having existed in the recent history of Mars. More broadly, this technique represents a potentially valuable tool within a GIS framework for increasing confidence in data/model comparisons at global, hemispheric and regional scales.

CHAPTER ONE: INTRODUCTION

1.1 Background

The field of planetary science, by necessity, must rely almost entirely upon remote sensing data to accurately decipher the physical processes that shape and modify the surfaces of terrestrial planets and satellites. An abundance of data returned by multiple missions has amplified the need for sophisticated management and analysis these data. This reality has gradually motivated the planetary science community to adopt geographic information science (GIS) techniques to extract as much information as possible from these data sets (Frigeri et al., 2011; Hare et al., 2012) and to manage them appropriately.

While the technology has changed, the overarching goals of studying the surfaces of planetary bodies has remained simple: (1) What surface features are of interest and where are they?; and (2) what process or processes created them? The first question is one that can be addressed by mapping, while the second question is situation-dependent. For planetary bodies that have atmospheres (Venus, Earth, Mars and Titan), modeling of the climate using general circulation models (GCMs) can yield predictions that can help assess whether specific climate-related processes are plausible explanations for surface features (e.g. Forget et al., 2006).

GCMs, most commonly used for terrestrial applications, have grown in popularity and in sophistication recently due to advances in computational capabilities and an increased appreciation of the sensitivity of Earth's climate. GCMs allow for detailed forecasting of atmospheric response to increased greenhouse warming and the potential environmental consequences over the scale of the next century (Satoh, 2013). At the

most fundamental level, GCMs solve equations for fluid dynamics that reflect flow within the atmosphere of a planet. On the Earth, the climate is so strongly influenced by the presence of oceans that distinct GCMs have historically been used: Oceanic GCMs for modeling the ocean and Atmospheric GCMs for modeling the atmosphere, with models that combine the two (Atmosphere-Ocean GCMs) representing the most sophisticated models that are used for terrestrial climate forecasting (IPCC, 2007).

Despite the fact that GCMs are powerful for reconstructing climatological histories and forecasting atmospheric evolution, their results are not easily appreciated without geospatial visualization. GIS is an effective visualization tool, but techniques designed for integrating surface mapping data with GCMs are primitive. Instead, qualitative correlations are inferred by analyzing the two types of data separately (Haberle et al., 2001; Forget et al., 2006; Madeleine et al., 2009; Kerber et al., 2012). Further, sophisticated mapping and database techniques, while available, have been employed in planetary GIS sparingly. This presents a valuable opportunity to modernize: (1) the collection of geospatial mapping data; and (2) the integration of climate and surface datasets within a GIS environment.

A natural scientific target for this type of integration are gullies on Mars (Figure 1), which are small channels that have been postulated to have been carved by liquid water (Malin and Edgett, 2000). Several details regarding the distribution of gullies on Mars strongly suggest that the climate of Mars plays a role in their formation (Malin and Edgett, 2000), and it is known that they are geologically young (active within the last one million years) (Reiss et al., 2004; Schon, Head, and Fassett, 2009), and are undergoing modification today (Diniega et al., 2010; Dundas et al., 2012). Given their morphologic
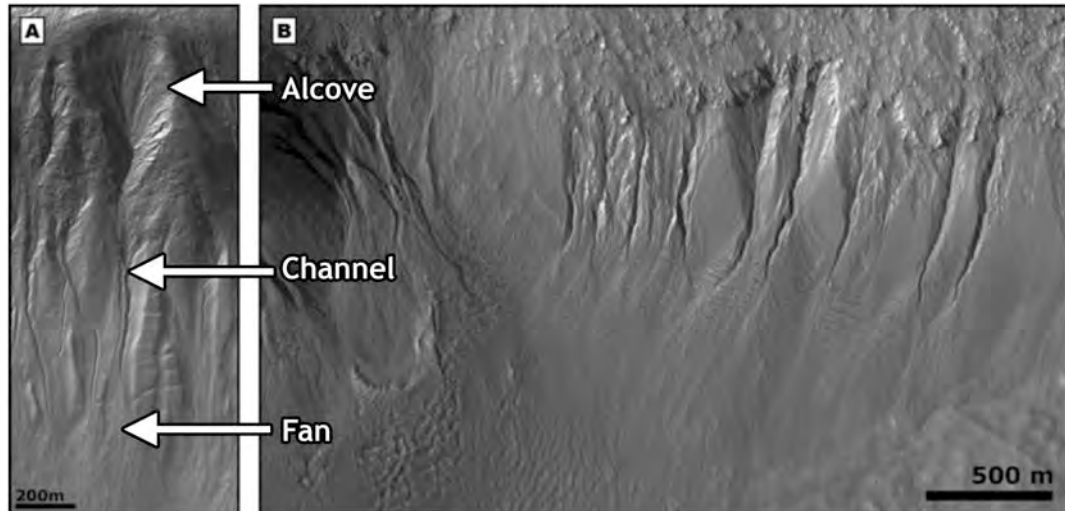
Figure 1 Sample of typical gullies on Mars. Classically, gullies consist of broad alcoves that taper downslope to a sinuous channel that leads to a depositional apron near the base of slope. Their visible similarity to water-carved channels on Earth has led to speculation that water has flowed on Mars in recent geologic history.

similarity to water-carved channels on Earth, gullies have frequently been used to argue that liquid water has flowed recently on the surface of Mars (Malin and Edgett, 2000; Heldmann and Mellon, 2004; Dickson and Head, 2009), in spite of extremely cold and dry conditions. If gullies are indeed formed by liquid water, this would have significant implications for the potential of primitive extant biology on the surface of another planet.

To date, GCMs have not been utilized to test whether liquid water could be present or could have been present in the recent history of Mars at locations where gullies are observed. The computational hardware and software resources required to answer this question quantitatively are now in place.

1.1.1 Gullies on Mars

Gullies are common in the mid-latitudes of each hemisphere on Mars (Milliken, Mustard, and Goldsby, 2003). They generally follow a simple morphological pattern with

3
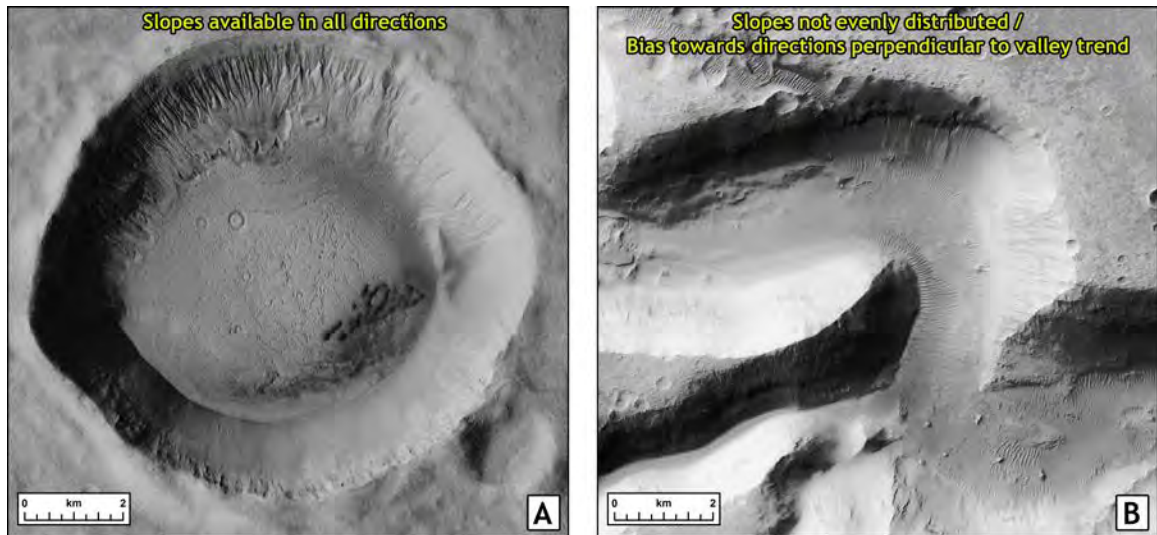
Figure 2 Gullies on impact crater vs. valley wall. (A) Gullies forming on the wall of a fresh impact crater in the southern hemisphere of Mars. Gullies are found preferentially on the pole-facing (northern) slope of the crater. (B) Gullies forming on the northern wall of Nirgal Valles in the southern hemisphere of Mars. Orientation measurements of gullies should not be made on this surface, since slopes are biased towards only north-facing and south-facing.

an alcove at the top of a slope which tapers to a constant-width channel, and a depositional fan at the bottom of the host slope (Figure 1) (Malin and Edgett, 2000). However, the intense targeting of the surface of Mars with orbital cameras such as Mars Orbiter Camera (MOC) (Malin and Edgett, 2001), the Thermal Emission Imaging System (THEMIS) (Christensen et al., 2004), the High Resolution Stereo Camera (HRSC) (Neukum et al., 2010), the Context Camera (CTX) (Malin et al., 2007), and the High Resolution Imaging Science Experiment (HiRISE) (McEwen et al., 2010) has revealed that they vary in their detailed morphology (Dickson and Head, 2009). Gullies fall into three general categories (Levy et al., 2009): (1) gullies with alcoves that erode bedrock; (2) gullies with alcoves that erode a softer mantling material; and (3) gullies that erode dunes. Further, the geologic feature upon which the gully forms is critical for successive
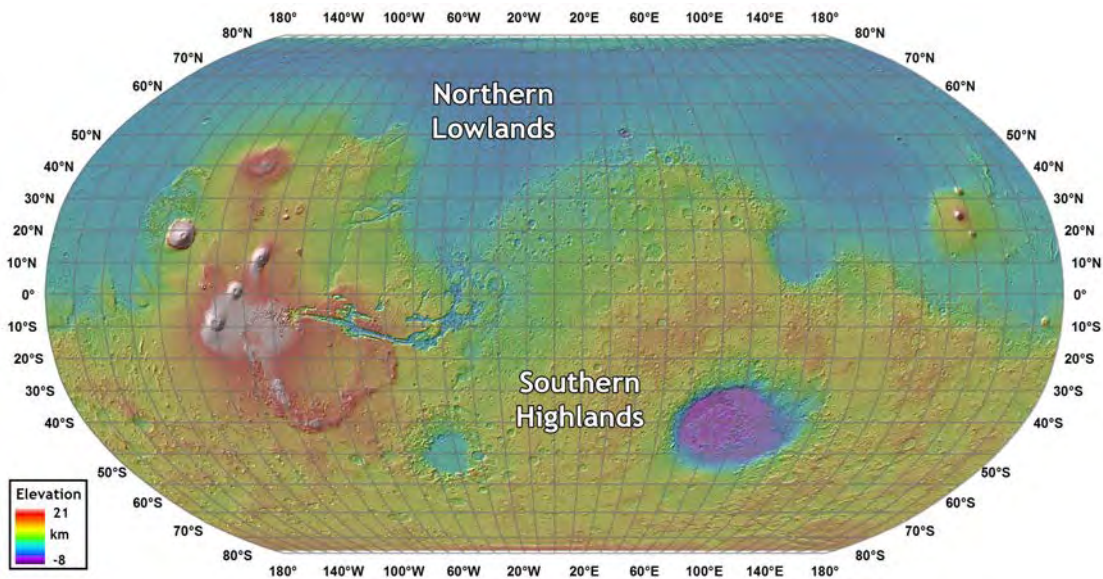
Figure 3   Global topography of Mars as measured by the Mars Orbiter Laser Altimeter (MOLA). The northern 1/3 of the planet is referred to as the "northern lowlands," in contrast to the "southern highlands." The northern lowlands are characterized by a paucity of steep slopes, due to resurfacing by fluvial and volcanic processes. Thus, there are not as many slopes available upon which gullies can form, as compared to the rugged southern highlands.

measurements that can be made from the gullies themselves. For example, an accurate and unbiased measurement of gully orientation can only be made by using gullies that form on slopes that sample all possible orientation directions (Figure 2). Fresh impact craters provide slopes at all 360° of orientation, so it will be necessary to create a subset of gullies, within a geodatabase, that includes only gullies on these slopes.

1.1.2 Mars' crustal dichotomy and slope availability

The crust of Mars exhibits a unique trait not observed on other planets: a *crustal dichotomy* (Zuber et al., 2000) where the northern third of the crust of the planet is considerably thinner than the remainder of the planet (Figure 3). The crustal dichotomy has caused almost complete erosion and resurfacing of the northern plains of Mars (the

"northern lowlands") by possible flood waters and lava (Kreslavsky and Head, 2002), such that almost all steep slopes that formed early in Mars' history have been buried or eroded north of the dichotomy boundary. In contrast, large craters with steep slopes in the *southern highlands* have been largely preserved (Figure 3). Large basins like Argyre and Hellas show resurfacing on their floors, but the majority of terrain in the mid-latitudes of the southern hemisphere contain slopes steep enough to initiate gully activity (Dickson, Head, and Kreslavsky, 2007).

1.1.3 Recent Climate of Mars

It is now known that the climate of Mars today is not representative of the climate over the last million years (Head et al., 2003), during which time gullies have been active (Reiss et al., 2004; Schon, Head, and Fassett, 2009). Like the Earth, Mars goes through significant eras of climate change that are likely to have dramatic effects on the stability of water at the surface (Laskar et al., 2004). Thus, simply modeling the present climate is not sufficient to characterize stability conditions at locations where gullies are observed.

Recent studies have concluded that the obliquity of Mars, which is the angle between the rotational axis that runs through the planet from the north rotational pole to the south rotational pole and the plane defined by the planet's orbit around the sun (Figure 4), varies significantly over relatively short geologic timescales (Laskar, Levrard, and Mustard, 2002; Laskar et al., 2004). Within the last million years, the obliquity of Mars reached a peak of 35° compared to its current value of 25°. The varying obliquity changes the regions where liquid water could exist on the martian surface, due to
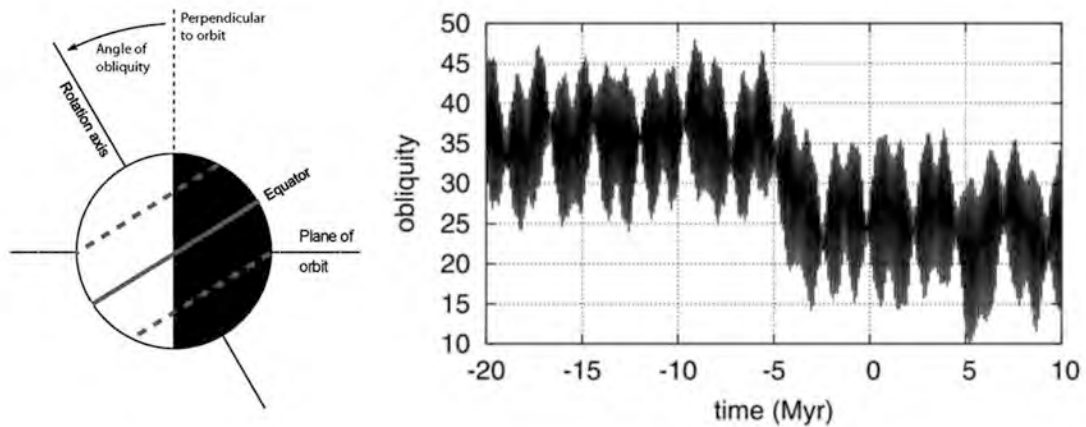
Figure 4 Obliquity diagrams. (A) Diagram showing how obliquity is calculated. 0° obliquity is when the rotation axis of the planet is perpendicular to the plane of the planet's orbit. 90° obliquity is when the rotation axis is parallel to the plane of the orbit. Thus, higher values of obliquity cause more energy from the sun to be imparted to the polar regions of the planet. (B) Calculations of obliquity in the recent geologic history of Mars (from (Laskar et al., 2004)). Relatively high obliquity conditions (35°) have been achieved within the last one million years, when gullies have formed on Mars.

increased insolation at higher latitudes increasing sublimation of surface volatiles in polar regions (Head et al., 2003).

High-obliquity conditions are also thought to have sublimated massive CO_2 ice deposits that are trapped in the south polar cap of Mars (Phillips et al., 2011). Simulations using a GCM crated by NASA's Ames Research Center (referred to as AMES-GCM here; see Section 1.2.2 for more details) predict that at 35° obliquity, this CO_2 reservoir would be released as a gas into the atmosphere, raising the average atmospheric pressure on Mars to ~10 mb, from ~6 mb at present under low-obliquity conditions (Phillips et al., 2011). Thus, there is a clear motivation for modeling the climate not just of present-day Mars, but also during these times when temperature and pressure conditions may have been different than what is observed today. GCM simulations should therefore explore three different starting conditions such as obliquity
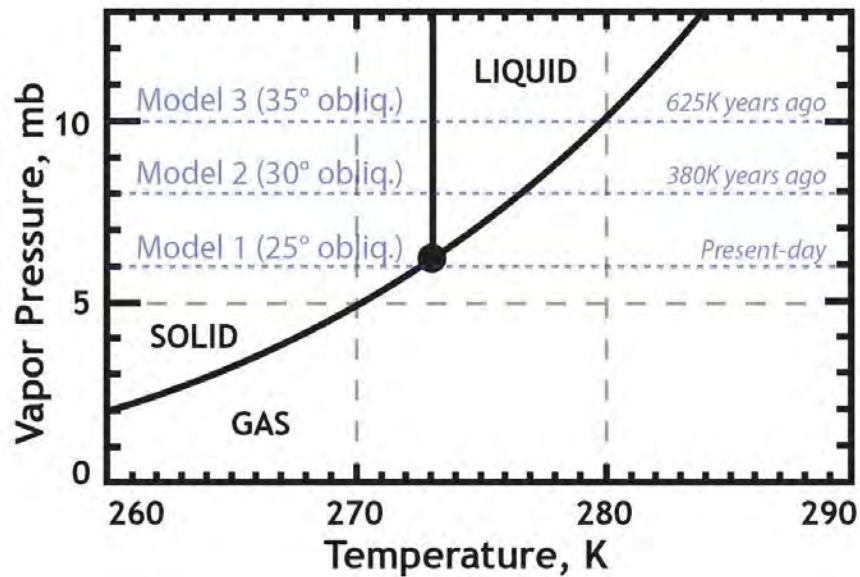
Figure 5 Phase Diagram for water. The triple point, where water could exist as any of the three phases of matter, occurs at T = 273.16 K and P = 6.11 mb. Surface conditions that surpass these values could, in principle, permit the existence of liquid water. Globally, conditions on Mars straddle this point, so determining which location meet both criteria at the same time is necessary for predicting possible locations for liquid water.

= 25° and average pressure = 6 mb, obliquity = 30° and average pressure = 8 mb, and obliquity = 35° and average pressure = 10 mb, since comparison of the results could provide a range of possibilities for liquid water stability on Mars.

1.1.4 Dynamic range of topography on Mars

The southern hemisphere provides a large range in elevation, which is a critical factor when attempting to assess stability conditions for liquid water at the surface. Mars, like the Earth, straddles the triple point of water (Figure 5), which represents the temperature and pressure conditions at which water could exist as a solid, liquid or gas. Since pressure changes as a function of altitude, elevation is a valuable first-order proxy for determining where liquid water could exist at the surface.

The vertical datum for Mars is the elevation where the pressure at the surface is equal to the triple point pressure for water, which is 6.11 mb. Thus, under current atmospheric conditions, surfaces below the datum could permit liquid water, while surfaces above the datum cannot (Figure 5). The southern hemisphere (poleward of 20°S) contains surfaces as high as ~8 km above the datum and as low as ~-8 km (Figure 3). Thus, mapping gullies in the southern hemisphere removes any potential bias of only sampling surfaces within a specific elevation window.

1.1.5 Objectives of this study

This study uses gullies (Malin and Edgett, 2000) to demonstrate the value of using geodatabases in planetary science and for the application of new tools designed to qualitatively and quantitatively compare mapping and GCM data. Geodatabases, within the ArcGIS 10.2 platform (Esri, 2014a), provide a format that allows for the characterization of an array of attributes of gullies within a geospatial framework, permitting efficient integration with GCM simulations.

Integration of GCM simulations and a geodatabase of gullies allows for a direct test of whether gullies occur in regions where the conditions for melting of H_2O ice is possible. To accomplish the geodatabase/GCM integration three goals must be achieved:

(1) A geodatabase of gullies in the southern hemisphere must be created using data from the CTX camera;

(2) GCM simulation results run at three starting obliquity conditions (25°, 30°, and 35°) of Mars must be successfully imported into GIS and verified as being properly registered;

9

(3) Automated routines must be developed to integrate the geodatabase with three GCM simulations results, providing a range of possibilities to investigate for liquid water stability on Mars.

Given the novel nature of this integration approach within GIS (both planetary and terrestrial), the volume of existing literature for this end-to-end process is low. However, prior studies of some of the individual components of this workflow provide a useful context for the motivation and methodology behind this study.

1.2 Literature Review

1.2.1 Cataloging morphological features on Mars and use of geodatabases

While several surveys of gullies on Mars have been conducted since their discovery (Malin and Edgett, 2000; Milliken, Mustard, and Goldsby, 2003; Heldmann and Mellon, 2004; Berman et al., 2005; Bridges and Lackner, 2006; Dickson, Head, and Kreslavsky, 2007; Heldmann et al., 2007; Wilson and Hamilton, 1996; Kneissl et al., 2010), none have been published in a GIS-ready format that could serve as a model for the most efficient way to map gullies. Additionally, published gully surveys have relied upon older datasets that were the best data available at the time but do not take advantage of the massive volume of data returned by the Mars Reconnaissance Orbiter (MRO) spacecraft since 2006, particularly via the CTX camera, which has provided the most substantial image source for mapping gullies (Malin et al., 2007).

Morphologically, the most similar large-scale mapping effort is the global catalog of valley networks on Mars published by Hynek, Beach, and Hoke (2010). Valley networks are larger dendritic valleys that date to early Mars history (Fassett and Head, 2008) and provide strong evidence of a more stable environment for liquid water ~3.7

billion years ago. Like gullies, valley networks are most appropriately mapped as linear features, making them potentially an attractive analog for this database structure. Made available through the Planetary Interactive GIS-on-the-Web Analyzable Database (PIGWAD) (Hare, 2014) online forum, the data are available as a stand-alone polyline shapefile that maps 9,879 features. The shapefile consists of one attribute, "tot_length," which represents the total length of each element within the shapefile. The geodatabase of gullies to be created here would have a wider array of attributes with multiple types of fields, so this template would not achieve this goal.

A more elaborate technique is being attempted by Hayward et al. (2012), who are currently undertaking the task of mapping every visible dune on the surface of Mars to decipher information about boundary layer dynamics of the martian atmosphere at the surface. They have published a catalog of dunes in the vicinity of the north pole that maps both individual dunes and the boundaries of dune fields themselves. Given the varying nature and scale of the features being mapped, a feature class within a geodatabase was created, with individual feature classes that map specific aspects of the features being mapped (average slipface direction, dune field perimeter, dune field centroid, etc.). This is not directly relatable to gullies, in that gullies are discrete objects that are only defined by one type of feature (polyline).

The most popular feature for large-scale mapping has been impact craters, the most ubiquitous surface feature in the solar system, and the only proxy available for determining absolute age estimations of surface features. For the Moon (Head et al., 2010) and Mercury (Fassett et al., 2011), all craters that measure greater than 20 km in diameter were mapped as polygons and collected within shapefiles. Physical attributes

11
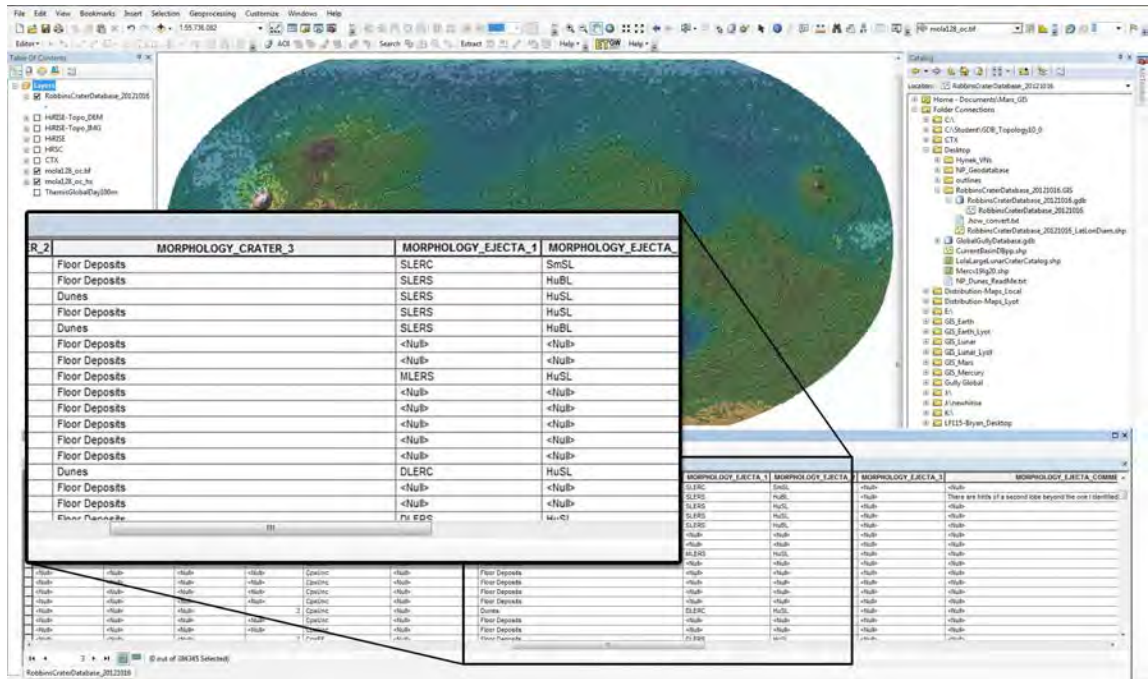
Figure 6 Sample geodatabase from crater catalog. Display of the geodatabase created by (Robbins and Hynek, 2012). The geodatabase structure permits efficient indexing of feature classes and coded domains allow for rapid creation and recall of string-based attributes (inset).

(diameter, latitude, longitude) were recorded, but no morphological classification scheme

for other parameters was included.

Alternatively, Robbins and Hynek (2012) published a massive geodatabase

(MRCTR, 2014) of every impact crater on Mars that is greater than 1 km in diameter,

totaling 384,345 individual craters. Each feature has an array of attributes that provides a

detailed characterization of the crater in question. While most of these attributes are

quantifiable physical properties that can be calculated after mapping, also included are

morphologic descriptive classifications that are valuable for sub-setting the final database

and are best determined during the mapping process. For instance, craters that contain

"dunes" can be partitioned from craters that only contain "floor deposits" (Figure 6). This

12

significantly extends the utility of the catalog and is analogous to the desired geodatabase of gullies on Mars in this study.

The structure used by Robbins and Hynek (2012) is a point feature class stored within a file geodatabase. Advantages of using a file geodatabase apply to both the collection of the data itself and the subsequent rendering and utilization of the data. First, to efficiently assign string-based morphologic descriptions to each feature, coded domains within a geodatabase allow for rapid assignment (choosing from a drop-down menu instead of manually typing descriptions) and a guarantee of consistency and coherence (elimination of typographical errors). Additionally, what is predicted to be the most common attributes can be assigned as defaults, significantly reducing the workload required for large-scale databases. Second, the geodatabase environment allows for efficient indexing of features and fast rendering of features with coded domains (Buckley, 2013; Childs, 2009). Finally, ArcGIS has gradually become the standard GIS platform for planetary science mapping (Hare et al., 2012), thus allowing for more efficient collaboration and comparison with other data sets.

1.2.2 General Circulation Models (GCM) for Mars

The success of several spacecraft missions to Mars has provided enough data to allow for modeling of the circulation of the atmosphere up to 80 km above the surface (Forget et al., 1999). This modeling includes robust predictions of boundary layer processes that dictate phase changes of volatiles on the surface of the planet. Since the atmosphere is comprised mostly of CO_2 and surface and near-surface ice deposits are mostly H_2O, the behavior and fate of these specific volatiles are the focus of many GCM simulations of

Mars. The lack of oceans on Mars simplifies the models such that predictions of present-day conditions are reliable and have been tested against remote sensing data (Christensen, 2000; Christensen et al., 2004) and measurements made by robotic landers that included meteorological instruments (Nier et al., 1976; Smith et al., 2009). Recent data from the Mars Climate Sounder, which obtains vertical profiles of atmospheric composition, have resulted in more robust simulations of the 3D dynamics of the atmosphere (McCleese et al., 2007). The lack of plate tectonics on Mars allows for these models to be applied to previous eras when the parameters that define Mars' orbit around the sun were different, with confidence that the topography of the surface was the same as it is today at the global scale.

Three primary Mars GCMs have been used in the planetary science community, constructed by the following institutions: (1) the Geophysical Fluid Dynamics Laboratory (hereafter GFDL-GCM) (Wilson and Hamilton, 1996); (2) Laboratoire de Météorologie Dynamique at the University of Paris (hereafter LMD-GCM) (Forget et al., 1999); and (3) NASA Ames Research Center (hereafter AMES-GCM) (Haberle, Murphy, and Schaeffer, 2003). To decipher the evolution of the water cycle on Mars, the LMD-GCM and the GFDL-GCM have both been used to predict net accumulation of H_2O ice at the surface in the mid- and low-latitudes of Mars in the Late Amazonian epoch (within the last few hundred million years). The GFDL-GCM has been used to assess the global stability of water ice as a function of latitude as Mars undergoes perturbations in its orbital parameters over time, suggesting that there were likely episodes in Mars' history when water ice was more stable in the near-surface at lower latitudes than it is today (Mischna et al., 2003). The LMD-GCM successfully predicted sufficient ice
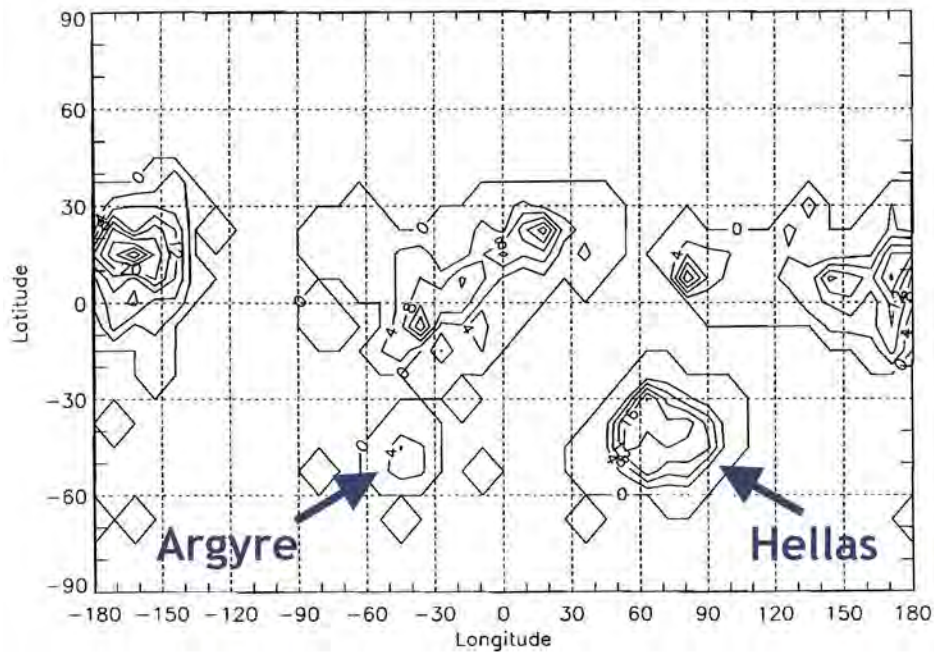
Figure 7 Previous attempt to model liquid water stability on Mars (Haberle et al. 2001). Contours represent the number of sols (martian days) where conditions surpass the triple point of water. Only Argyre and Hellas impact basins support transient liquid water in the southern mid-latitudes.

accumulation due to adiabatic cooling for glacial flow on the western flanks of the Tharsis Montes and in eastern Hellas (Forget et al., 2006), correlated with features that had been mapped as cold-based glacial deposits (Lucchitta, 1981; Head and Marchant, 2003; Shean et al., 2007; Shean, Head, and Marchant, 2005; Pierce and Crown, 2003; Head et al., 2005).

Only the AMES-GCM, however, has been used to determine the potential for liquid water on the surface of Mars under present-day conditions (Haberle et al., 2001) (Figure 7). This study subdivided Mars into a grid of cells and determined for how many *sols* (martian days) were conditions above the triple-point of water, such that the temperature surpasses 273° K and pressure surpasses 6.11 mb, thus allowing for liquid water to exist at the surface. According to the AMES-GCM model, under present

conditions, only along the rims and on the floors of the giant impact basins (Argyre and Hellas) could water potentially exist at the mid-latitude locations where gullies are found (Figure 3) (Malin and Edgett, 2000).

This study uses the LMD-GCM to simulate H_2O stability conditions for three different starting conditions, including those that represent present-day Mars. Thus, the results from the AMES-GCM analysis (Haberle et al., 2001) provide an independent product against which the results of this current analysis can be compared. Haberle et al. (2001) also highlight several drawbacks of a GCM-only approach that can be addressed with GCM-GIS integration: (1) lack of a morphologic basemap to provide context; (2) lack of connection between modeled climate predictions and specific morphological surface features, gullies in the present case; and (3) lack of visualization of the dynamics of the modeled climate over time. With modern GIS capabilities, these limitations can now be avoided.

1.2.3 Importing of GCM results into compatible GIS formats

Incorporation of GCM simulations into GIS historically has been computationally limited, as processing capacity within GIS software was not very efficient at performing tasks on data sets that are global in extent (Streit and Wiesmann, 1996). Further, GIS was initially viewed by some as an environment within which the modeling itself would be performed, as opposed to a framework for storage and rendering of model results (Steyaert and Goodchild, 1994). While some modeling tools currently available within GIS packages resulted from this approach, larger scale models required computational resources that exceeded the computational limitations of desktop GIS architectures.

Thus, GIS and GCMs were used in conjunction with each other but not fully integrated in a way that would facilitate quantitative analysis (Goodchild et al., 1996). Progress was also significantly slowed by a lack of interest within the modeling community and the steep learning curve associated with GIS during this time (Albrecht, 1996).

More localized studies, however, were conducted that revealed the potential inherent in more fully integrating GIS and model simulations (e.g. Bivand and Lucas, 2000). Once computational resources became sufficient for managing global data sets and GIS became more accessible to non-GIS specialists, studies were conducted that imported GCM outputs as linked point layers that provided immediate access to model runs within a GIS interface (Akinyemi and Adejuwon, 2008). At this same time, Esri introduced support for the Network Common Data Form (netCDF) file standard with a suite of conversion tools that allow for importing and exporting of multi-dimensional data (Esri, 2007). Given its strength at efficiently handling multi-dimensional data, netCDF (Rew and Davis, 1990), a machine-independent data format that supports the creation, access, and sharing of array-oriented scientific data, has become the dominant output format for GCM results. This format allows one file to contain all of the parameters for a simulation (surface temperature, pressure, etc.) in a spatial context, but also with a time dimension, as opposed to having discrete files for each individual time step.

Gradually, interest within the GIS community for importing netCDF-based climate simulations has increased for both the ArcGIS community (Noman, Zimble, and Sigwart, 2013) and the OpenGIS community (Koziol, 2013). Because the data to be integrated with the GCM results is stored in ArcGIS, focusing on methods for migrating GCMs to ArcGIS is important. With support for netCDF now available within ArcGIS,

most GCM simulations can now be read as a table, feature or raster. Small proof-of-concept examples investigating soil moisture (Xiaolong, 2012) and weather visualization (Xiong and Wang, 2010) have provided a template for how these data can now be accessed within GIS and potentially used for surface condition assessments at specific locations on Earth.

1.2.4 Automating the integration of GCM outputs and surface data in a GIS

To date, no peer-reviewed literature exists that has achieved the goals of this study: (1) to generate GCM/data animations over time within GIS; and (2) to extract values from GCMs at specific locations in an automated routine. There are, however, several tutorials and demonstrations online that show how to create animations using the time field within a specified layer and the animation toolset within ArcGIS (Whiteaker, 2006; Telis, 2007; Esri, 2014b). This provides a template for accessing all time steps of the input data set, but not necessarily integrating it fully with the companion geodatabase.

An alternative to using the ArcGIS animation toolset is to export successive maps as images that can then be compiled into an animation using third-party software that is more specialized for rendering movies and provides more dexterity for this type of visualization. This can be accomplished in an automated fashion by using a Python script that iterates through time steps within the netCDF file, as is described in Chapter 3 and Appendix A.

For extracting quantitative data from GCMs at specific locations derived from a separate geodatabase, to date there is no literature available that proposes a way to achieve this portion of the workflow in an automated way. Thus, a novel contribution of

this work, as described below, is the generation of a Python code that extracts specific values from a GCM output at specific sites within a geodatabase (Appendix B). While this is computationally intensive, it allows for an assessment of conditions at these sites across the entire planet.

CHAPTER TWO: STUDY AREA

The northern and southern hemispheres of Mars differ in both their physical properties and how they experience seasons depending upon specific astronomical properties of Mars' axial tilt and its orbit around the sun. A brief summary of these factors is important for understanding the physical constraints placed upon the survey outlined in the methods section (Chapter 3) and the results when the survey is integrated with the GCM simulations (Chapter 4).

2.1 Physical characterization of the southern hemisphere of Mars

Gullies are found in the mid- and high-latitudes ($> 30°$) of each hemisphere on Mars (Malin and Edgett, 2000). Thus, terrain within 20° of the equator were not considered for this study. Comparing the two hemispheres, there are considerably more gullies in the south (Malin and Edgett, 2000; Milliken, Mustard, and Goldsby, 2003), and there are two possible explanations for this that are not mutually exclusive:

(1) Steep slopes, required for gully formation (Dickson, Head, and Kreslavsky, 2007), are more common in the southern hemisphere.

(2) The orbit of Mars around the sun is more elliptical than that of the Earth, such that winters in the southern hemisphere are long and cold, while summers are short but relatively warm, warm enough to melt H_2O ice. The northern hemisphere, under current conditions, does not experience this high-amplitude annual variation.

2.1.1 Elevation, slope distribution and orientation

The crustal dichotomy of Mars separates the surface into two major units: the northern lowlands and the southern highlands (Figure 3). The exact cause of this dichotomy has been proposed to be either due to unusually vigorous mantle convection focused under the northern plains that weakened the overlying lithosphere (Zuber et al., 2000) or a giant impact soon after planetary formation (Andrews-Hanna, Zuber, and Benerdt, 2008). Regardless of the cause, the topographically low nature of the northern plains resulted in it serving as a hemisphere-scale basin for both flood volcanism and sediments transported through massive outflow channels to the south (Kreslavsky and Head, 2002).

This activity eroded and buried almost all of the impact crater population from the Noachian (the first several hundred million years of Mars' history) in the northern hemisphere, a record that is still preserved in the southern highlands. On a planet that lacks plate tectonics, impact craters provide the most abundant source of steep slopes, which are required for gully formation, as gullies rarely form on slopes more shallow than 20° (Dickson, Head, and Kreslavsky, 2007). This disparity in steep slope availability is most clearly visualized in global roughness maps using Mars Orbiter Laser Altimeter (MOLA) data (Figure 8) (Kreslavsky and Head, 2000).

Steep slopes are also provided by the walls of valley networks. Their distribution is strongly correlated with Noachian terrain (Hynek, Beach, and Hoke, 2010) that is almost entirely restricted to the preserved southern highlands and has been buried or eroded in the northern lowlands. Thus, local topography on Mars is strongly biased towards forming gullies in the southern hemisphere instead of the north. This helps to provide greater statistics for comparison with GCM results.

21
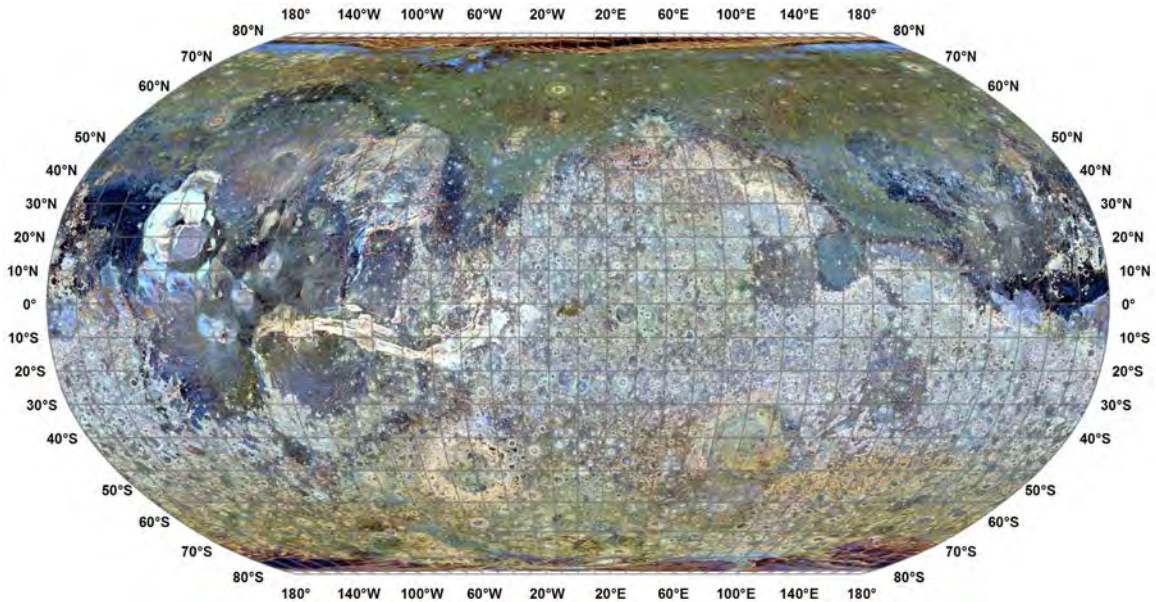
Figure 8 The global roughness of Mars. Roughness values were calculated for three different along-track baselines and mapped as separate color channels: Red (0.6 km), Green (2.4 km) and Blue (19.2 km) (from Kreslavsky and Head, 2000). Lighter tones represent rougher topography while darker tones denote smoother topography. Impact crater walls provide the majority of steep slopes on Mars, thus the northern lowlands have uniformly smooth terrains while the southern highlands have high-frequency steep slopes conducive to gully formation.

2.1.2 Seasonal disparity on Mars and implications on GCM analysis

In addition to the contrast in the availability of steep slopes, the two hemispheres experience considerably different climate conditions as a function of astronomical forces. The orbit of Mars around the sun is considerably more elliptical than that of the Earth, such that it is 42.6 million km closer to the sun at its closest approach (perihelion) than at its greatest distance (aphelion). For scale, this difference for Earth is only ~5 million km. Since planets orbit the sun at a faster rate at perihelion and receive more solar energy during this period, this means that the hemisphere that experiences summer during perihelion has a very warm but very short summer and a very cold and very long winter. On Earth this effect is minor, but it is far more important on Mars, which has the second

22

most eccentric orbit in the solar system. The hemisphere that experiences short intense summers and long cold winters changes over time as the orbit of Mars precesses, but at the present time the southern hemisphere is subject to these conditions. Thus, the southern hemisphere provides a more dynamic environment for GCM analysis with more potential for phase changes of surface H_2O.

This has important implications for the stability of H_2O as an ice at the surface or as a liquid and is important for understanding the GCM results presented in Chapter 4. Since, under current conditions, the southern hemisphere experiences long, cold winters and short, warm summers, it is both the hemisphere that is most capable of accumulating ice on the surface during the winter (Madeleine et al., 2013) and most capable of melting ice on the surface during the summer. As the orbit of Mars precesses over tens of thousands of years, changing the critical orbital parameters that govern climate conditions at the surface, gully formation in the north was more likely during periods when the northern hemisphere experienced these high-amplitude seasonal conditions.

CHAPTER THREE: DATA AND METHODS

An integration pipeline is required to successfully merge GCM simulations and geodatabases. In this chapter, the three principal components of the GCM/geodatabase integration pipeline are described: (1) CTX image processing and geodatabase creation/mapping; (2) GCM generation and inclusion in ArcGIS; and (3) automation of integration procedures.

3.1 Geodatabase data and architecture

Because the CTX camera provided all of the data upon which the geodatabase in this study is based, it is worth providing detail regarding the pipeline required to convert raw spacecraft data to georeferenced image data within ArcGIS.

3.1.1 CTX data

CTX is actively acquiring high-resolution imagery of the martian surface while onboard the NASA MRO spacecraft. Four factors make it an ideal system for mapping gullies on Mars: (1) resolution (~6 m/px); (2) coverage (each image spans ~30 km in width); (3) wavelength captured (500-800 nm); and (4) acquisition timing (because MRO is in a sun-synchronous orbit, most images are acquired in late-afternoon local time, providing ideal illumination geometry for mapping morphological features). While other cameras provide higher resolution (High Resolution Imaging Science Experiment (HiRISE) (McEwen et al., 2010), Mars Orbiter Camera (MOC) (Malin and Edgett, 2001)), these datasets are not capable of providing the spatial coverage required for deciphering the global distribution of gullies. As of 2010, CTX had imaged over 50% of the planet

(Malin, 2010), with a large amount of redundant coverage to accommodate stereo imaging, change detection and poor imaging conditions. For many instances, multiple images of the same site were used to perform accurate mapping of gullies.

Each CTX image is posted to the Planetary Data System (PDS), a centralized online data archive funded by NASA and stored (in the case of CTX) at both the Jet Propulsion Laboratory (JPL) and the United States Geological Survey (USGS). CTX files are provided in a "raw" PDS format, with the extension .IMG. This file contains both the image data itself and a label file in its header that includes spacecraft ephemeris data regarding when the spacecraft acquired that specific image. These ephemeris data provide the link that allows for the image data to be properly georeferenced.

The PDS raw file is imported into the linux-based Integrated Software for Imagers and Spectrometers (ISIS) program, built and maintained by the USGS. ISIS provides the following tools to georeference raw spacecraft image data: (1) converts raw PDS .IMG files to the ISIS .cub format; (2) radiometrically calibrates the image based upon known camera parameters; (3) attaches spacecraft pointing data to the file based upon when the image was acquired; and (4) projects the image using the spacecraft pointing data to a user-specified coordinate system and orthorectifies it based upon available topography. While the .cub file produced is readable in ArcGIS, volume constraints make it advisable to compress the image and reduce the bit depth to 8-bit. For this, the linux routine 'gdal_translate' is able to convert .cub files to standard TIFFs with world files, with each image being rendered with a 2% standard deviation stretch. Along with the projection information, this allows CTX data sufficient for the mapping of gullies to be imported into ArcGIS. Batch processing using the High-Performance Computing cluster at Brown

University allowed for this procedure to be performed on all CTX images of Mars, including all images between 20° and 90°S.

A map of CTX image distribution was created as a polygon feature class that shows where each image is found on the surface of Mars, based upon tables of spacecraft data provided by the CTX team. A Python script was created to automatically load the image that corresponds to the footprint of interest, based upon user selection.

For this survey, the 20,835 images acquired between 20° and 90°S were scanned to determine whether or not gullies were present. Of these, 3,697 were determined to have evidence for gullies, and these images were used for mapping.

These processing techniques, developed through the effort of multiple organizations such as NASA and the USGS, were available for this project and provided the necessary context and tools for the specific method used for mapping gullies on Mars.

3.1.2 Geodatabase architecture

A geodatabase of gullies in the southern hemisphere was created to enable the mapping and cataloging of the increasingly complex morphology that has become more apparent with each successive mission sent to image the surface of Mars. Morphologic trends could be potential indicators of the conditions required to generate gullies. Based upon previous surveys and parameters predicted to be relevant, the following attributes (Table 1) were documented: (1) latitude; (2) longitude; (3) orientation; (4) elevation' (5) alcove type; and (6) host feature.

Though not discussed in this specific study, a separate type of feature related to gullies, inverted gullies (Dickson, Head, and Barbieri, 2013), were also cataloged as part

of this project. These features are sinuous ridges that form on similar slopes as gullies (sometimes the same slopes) and may represent older generations of gully activity that have since been inverted (Dickson, Head, and Barbieri, 2013). By this process, coarser material on the channel floor is preserved while fine-grained material that makes up the channel walls is removed by sublimation and wind. These features may be remnants of more ancient generations of gully activity and may serve as an input to future GCM/data integration projects.

For gullies themselves, a polyline feature class is sufficient to calculate the attributes that have been designated (Table 1). Three of the attributes (Latitude, Longitude and Elevation) can be calculated from the midpoint of each gully segment. One attribute (Orientation) relies upon the dimensions of the polyline itself and is dependent upon the specific projection being used to map the feature. Thus, calculations for orientation will be performed in Mercator, which preserves angle. For convenience, this is the native projection for the polyline feature class.

Table 1 Attributes for gully geodatabase

Attribute	Units	Data Type
Latitude	Degrees	Double
Longitude	Degrees	Double
Orientation	Degrees from north	Double
Elevation	Meters relative to datum	Double
Alcove Type	N/A	Text
Host Feature	N/A	Text

The final two attributes (Alcove Type and Host Feature) are text strings that provide morphological classifications that will allow for further partitioning of the complete geodatabase (Table 2). "Alcove Type" separates gullies that form within pre-existing bedrock alcoves ("Bedrock") from those that form entirely within a consolidated ice-rich draping unit common in the mid-latitudes, referred to in the database as "Latitude Dependent Mantle" (LDM). "Bedrock" alcoves are common at all latitudes on Mars independent of gully activity (Dickson and Head, 2009), while "Latitude Dependent Mantle" is, as its name suggests, only found at mid- and high-latitudes (Head et al., 2003), where gullies occur (Malin and Edgett, 2000). In examples of gullies with alcoves that form in a hybrid of bedrock and LDM, an "Undetermined" option must be made available to prevent mistaken classification.

Table 2 Criteria for Alcove Type attribute

Alcove Type	Code	Criteria
Bedrock	Bdr	Rocky margins at the top of a slope; amphitheater shape with high boulder density; low length-to-width ratio.
Latitude Dependent Mantle	LDM	Sharp cuspate margins; polygonal ground at the surface; high length-to-width ratio.
Undetermined	Und	Shares characteristics of both Bedrock and Latitude Dependent Mantle.

The attribute "Host Feature" will allow for further classification of gullies based upon the geologic feature upon which they form. This is important for several reasons. First, as discussed above, unbiased orientation measurements, which could reveal thermal properties specific to gullied slopes, cannot be made on surfaces where not all slope orientations are represented (Figure 2). This can only be accomplished on intact impact crater rims that have slopes facing all directions, thus a "Crater Rim (Full)" option must

be available. Second, gullies on some surfaces tend to have different specific morphologies than gullies found on other surfaces. For instance, gullies on dunes (Diniega et al., 2010) exhibit leveed channel margins and debris snouts at their terminus instead of broad fans. For future investigation of these specific features, it is necessary to segregate them in this survey not as a separate feature class but as a subset of the gully database as a whole. To encompass the spectrum of surface types upon which gullies form, the following options are available: (1) Crater Rim (Full); (2) Crater Rim (Insufficient); (3) Dune Face; (4) Valley Wall; (5) Polar Pit; or (6) Mesa. Table 3 describes the criteria necessary for the classification of these feature types.

Table 3 Criteria for Host Feature attribute

Feature Type	Code	Example	Criteria
Crater Rim (Full)	CRf		The impact crater is (1) completely intact along the rim (not breached), (2) imaged entirely by CTX in one or more frames, and (3) has illumination conditions sufficient for gully mapping.
Crater Rim (Insufficient)	CRi		Clear evidence that the feature is an impact crater but (1) the rim is breached, or (2) the crater is only partially imaged, or (3) the crater is imaged but not of sufficient quality or suitably illuminated to make detection possible at all locations.
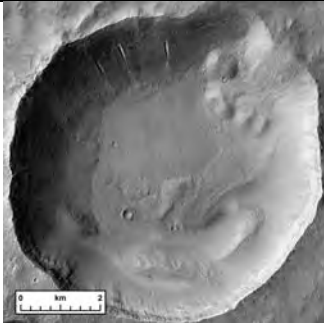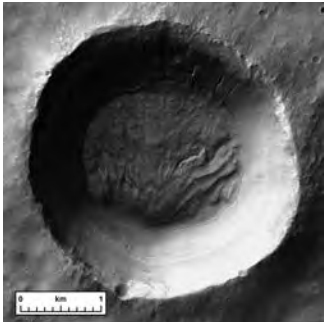
Table 3 (cont.)

Feature Type	Code	Example	Criteria
Dune Face	Dun		Substrate is extremely smooth with well defined ridge crests; frequently found in dense fields of dunes.
Valley Wall	Vly		Linear trough with parallel opposing walls.
Polar Pit	Ppt		Smooth-walled pits with sharp crests observed only in very high-latitude terrains.
Mesa	Msa		Any isolated topographically high feature (central peak, butte, etc.)
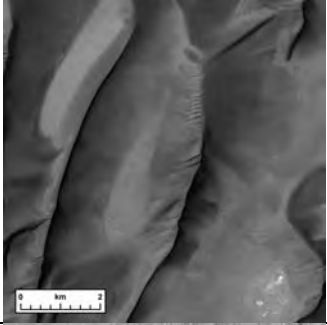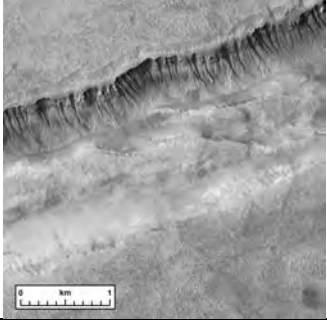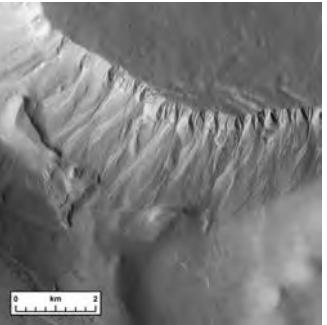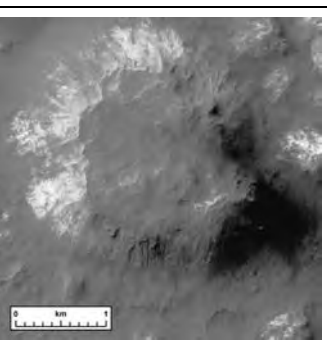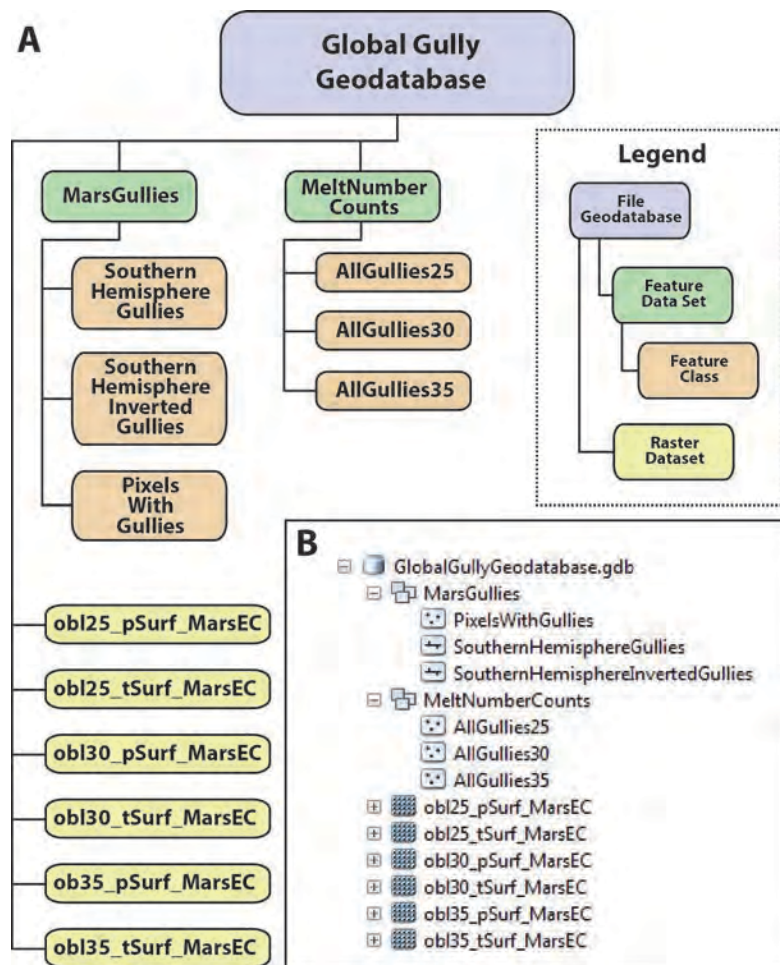
Figure 9 Geodatabase structure. (A) Schematic of the geodatabase design. Feature classes are divided into an input feature data set ("MarsGullies") and an output feature data set ("MeltNumberCounts"), which are the products of the GCM extraction python script. GCM outputs are stored as multi-band rasters based upon the starting conditions of the model run (i.e. obliquity) and the parameter represented (pressure (p) or temperature (t)). (B) Screenshot of the geodatabase within Catalog after the extraction routine has been performed.

Since these morphologic attributes are being stored as TEXT strings, three aspects of their incorporation take on amplified importance: (1) efficiency with regard to inputting the data; (2) consistency among values; and (3) defining default values that are the anticipated most popular attributes. These factors motivate the use of coded domains within the geodatabase structure. Each gully that is mapped is automatically assigned a value for Alcove Type (default = Undetermined) and Host Feature (default = Crater Rim

(Full)). Should these values require modification, the descriptions of the coded domain values are available for rapid alteration. For clarity, feature classes that represent the distributions of both gullies and inverted gullies are stored within a "MarsGullies" feature dataset within the geodatabase (Figure 9).

This geodatabase structure facilitated the mapping of 14,719 gullies in the southern hemisphere of Mars and 521 inverted gullies.

3.2 GCM simulations and incorporation into ArcGIS

Three separate LMD-GCM simulations were performed in support of this project under different starting conditions thought to have occurred on Mars during the last million years (Laskar, Levrard, and Mustard, 2002), as presented in Table 4.

Table 4 Input parameters for GCM simulations

Model name	Obliquity (deg)	Average surface pressure (mb)	Last time conditions occurred
06mb_25obliquity.nc	25	6	Present Day
08mb_30obliquity.nc	30	8	~380,000 years ago
10mb_35obliquity.nc	35	10	~625,000 years ago

Source: Age calculations from (Laskar, Levrard, and Mustard, 2002)

LMD-GCM simulation outputs were provided in three separate netCDF files (.nc), each containing a grid of cells that span the entire planet. Each cell: (1) spans 5° of longitude and 3° of latitude; (2) records values for seven model fields; and (3) records these values at 5,352 separate time steps, which corresponds to 8 records per sol (Mars day), over ~669 sols (one Mars year).   This temporal resolution is sufficient for deciphering diurnal patterns in temperature and pressure across the surface. Each simulation begins at the start of northern hemisphere spring (Solar Longitude (L_s) = 0°).

Of the seven values provided, the two of interest for this study are surface temperature and pressure. Four of the other five parameters are provided for quality assurance of the model, and the last provides an estimate of CO_2 ice on the surface.

Using the Multidimensional Toolbox in ArcGIS, the "Make NetCDF Raster Layer" tool was used to migrate each simulation into ArcGIS. Each simulation was imported twice, once for each variable of interest, in this case Temperature and Pressure. To accommodate the time steps embedded within the netCDF file, each time step was imported as a separate band for the resultant raster layer. The raster layers were then imported as multi-band rasters into the geodatabase (Figure 9).

A structured naming scheme was devised for the rasters that represent the GCM simulations. This was done to provide clarity and to facilitate the automated tasks that would be required to summon these files based upon designed input parameters. Each raster is unique based upon two specific criteria: (1) the obliquity value that defined the starting conditions for that model run (25°, 30° or 35°); and (2) the measurement of interest (temperature or pressure). Thus, these data needed to be included in the naming structure. A scheme with the format obl*XX*-*y*Surf.tif was used, in which *XX* represents the two-digit obliquity value for that model run, and *y* represents which measurement the file contained (t = temperature, p = pressure) (Figure 9). Obliquity was chosen instead of average pressure since this is a more intuitive variable for planetary scientists, and because the average pressure is a dependent variable that was derived from the AMES-GCM model based upon changing obliquity, an independent variable (Phillips et al., 2011). As an example, a raster that contained temperature values through a martian year with obliquity = 30 was stored as obl30-tSurf.

The "Make NetCDF Raster Layer" tool, by default, assigns the WGS1984 coordinate system to the imported data. Therefore, each raster layer must receive a geographic transformation from WGS1984 to Mars2000, which is defined by an equatorial radius of 3,396,190.0 m, and a polar radius of 3,376,200.0 m. Once this process was completed, individual bands from the rasters were added to a map document set using the Mars2000 datum to ensure proper registration. Major surface features discernible in the temperature/pressure data were found to register with controlled base maps of Mars at all latitudes, which provide the control network for CTX imagery. Thus, values extracted from these data will be accurate for the locations in question.

3.3 Automation of geodatabase/GCM integration

The quantitative extraction of LMD-GCM values at gully locations can help answer direct questions: (1) Did this gully experience melting conditions during this climate scenario?; (2) Did this gully experience melting conditions more often than nearby gullies?; and (3) What this technique provides in certainty it loses in context, in that it is more difficult to decipher exactly how the atmosphere behaves at these locations. For this, a qualitative visualization of atmospheric dynamics viewed in the context of gully locations provides a more holistic understanding of why gullies may form where they do, not simply whether they form by liquid water or not.
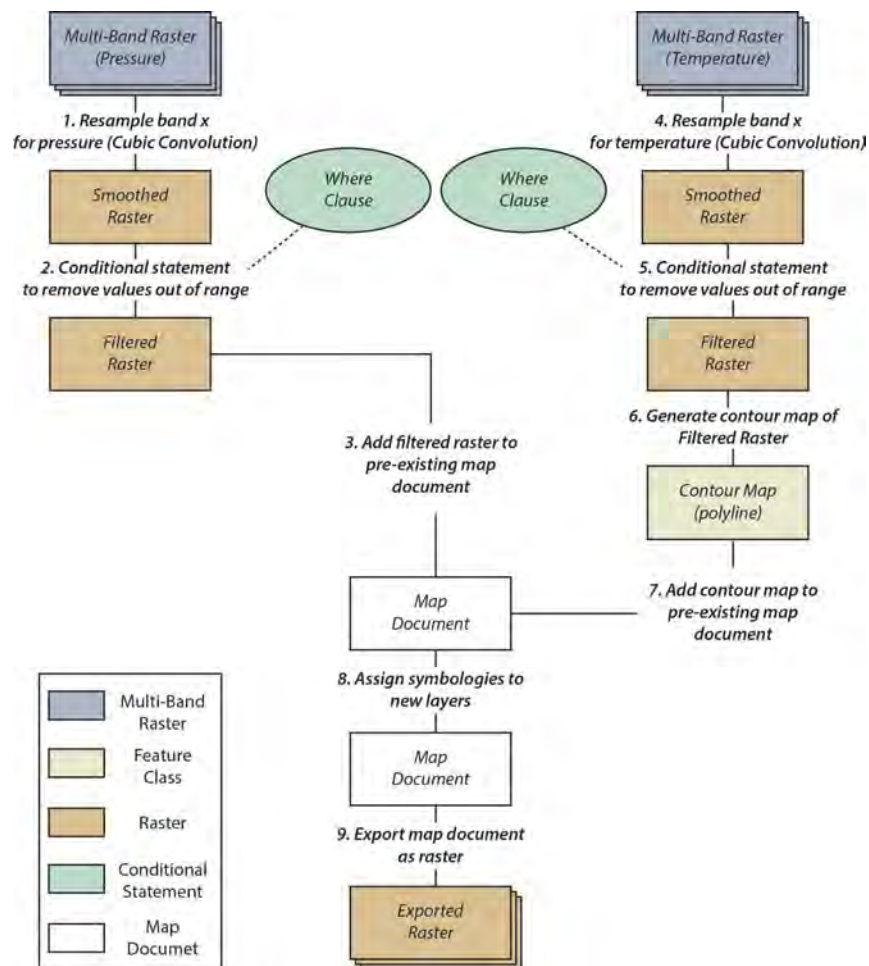
Figure 10 Schematic for animation script. Flow chart diagramming the pipeline to generate custom animations that link the geodatabase of gully locations (contained in the pre-existing map document) and the GCM simulation results for temperature and pressure. The process is iterated through every band contained in the input multi-band rasters that are derived from the GCM simulation.

3.3.1 Qualitative rendering of GCM/gully relationships

To generate animations using the time steps in the GCM results as a time variable, a stand-alone Python script was written that processed GCM data (both temperature and pressure) and plotted them both simultaneously on an existing map document that displayed the gully geodatabase. Since the goal of this process is to decipher which gully locations experienced melting conditions, several processing steps were necessary to

filter the plotted GCM data to focus only on areas that are: (1) greater than 273° K in temperature; and (2) greater than 6.11 mb in surface pressure. The following generalized steps were taken for each time step to produce the frames that subsequently are compiled into a yearlong animation, as shown in Figure 10:

(1) Resample band x for pressure (Cubic Convolution);

(2) Conditional statement to remove values out of range;

(3) Add filtered raster to pre-existing map document;

(4) Resample band x for temperature (Cubic Convolution);

(5) Conditional statement to remove values out of range;

(6) Generate contour map of filtered raster;

(7) Add contour map to pre-existing map document;

(8) Assign symbologies to new layers; and

(9) Export map document as raster.

Once this workflow was iterated over all 5,352 bands contained in each GCM simulation, an animation was created using third-party rendering software.

3.3.2 Quantitative extraction of temperature/pressure conditions at gully locations

A Python script was written to generate a feature class corresponding to the value "N," the number of times during the model run that that site experienced conditions above the triple point. This process, summarized in Figure 11, involves nine processing steps as summarized below:

1) Extract GCM based upon query, Convert to multi-band tiffs;

2) Create fishnet based upon resolution of GCM;

3) Extract feature class based upon query;

4) Select polygons which contain feature class;

5) Convert polygons to points (based on center);

6) Extract X & Y from multi-band tiff at each point; Iterate through points/bands;

7) Select rows where X & Y satisfy conditional statement; Iterate through geodatabase; compile to one feature class;

8) Count features by ObjectID (N); and

9) Join by ObjectID.
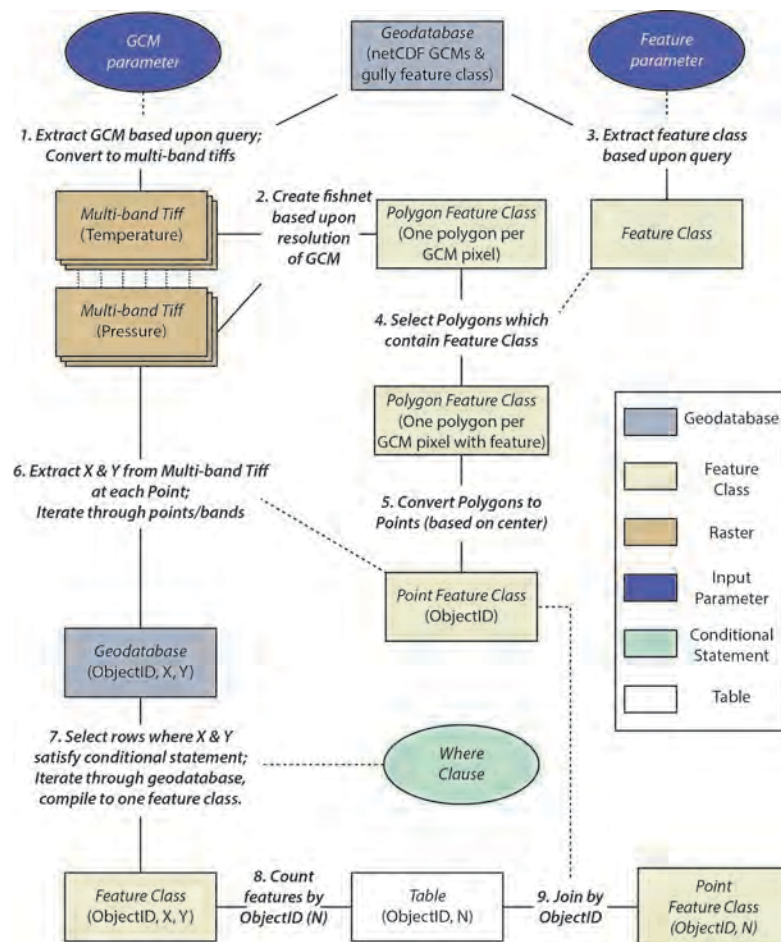
Figure 11 Schematic for quantitative extraction. The process is iterated at two levels: (1) values are extracted at a feature location from every band; and (2) this is done at every feature location. The final product is a point feature class that records the number of time steps when each site experienced melting conditions.

CHAPTER FOUR: RESULTS

These processes produced a wealth of new information about gullies on Mars and the climate that contributed to their formation. The results are presented in two primary sections: (1) Updated distribution properties of gullies and gully subtypes based upon parsing of the geodatabase; and (2) assessments of gully stability when analyzed in the context of LMD-GCM simulation results.

4.1 Updated distribution properties of gullies in the southern hemisphere

The geodatabase generated as part of this study provides the highest volume catalog of gullies in the southern hemisphere of Mars yet created. Further, the coded domains that were implemented from the outset allow for the partitioning of gullies based upon "Alcove Type" and "Host Feature," which facilitate a higher fidelity understanding of the complex distribution patterns of gullies, which could reflect important climatic processes.

4.1.1 Gully distribution as a function of latitude

This survey included all CTX images poleward of 20°S. The northernmost gully that was recorded is located at -27.91°S (Figure 12), which serves as an important latitudinal boundary for the conditions necessary to generate gullies on Mars, as there are no other climate-related variables that would preclude gully formation north of this location (slope, elevation, etc.). When classified by host feature (Figure 12), it is observed that the majority of gullies that occur equatorward of 30°S are found on valley walls, which is anomalous for the distribution of gullies as a whole. These gullies on valley walls are found on the walls of Nirgal Valles, an ancient valley network formed in the early portion
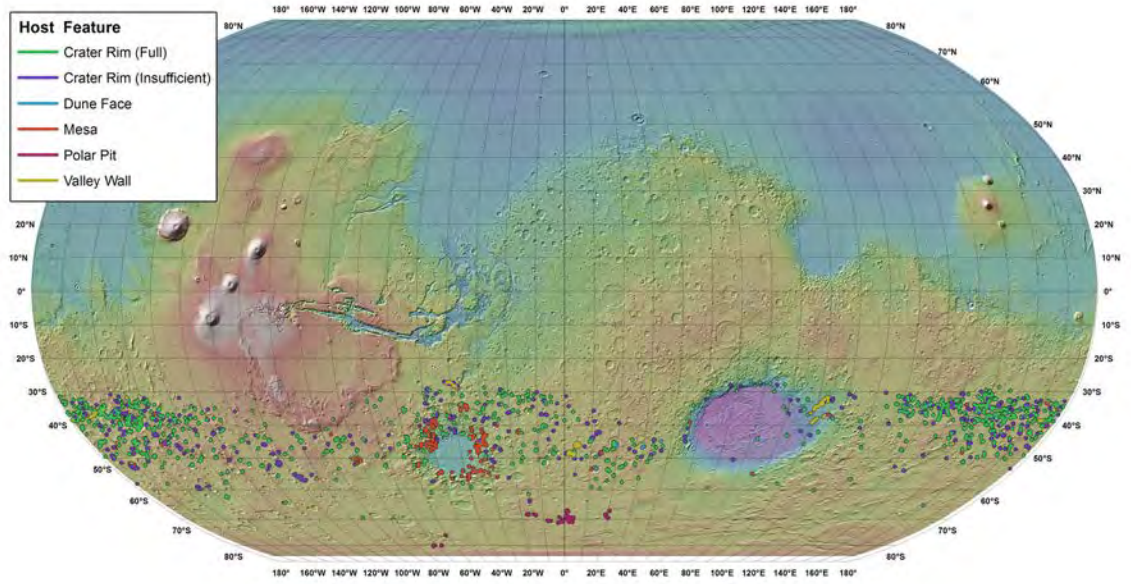
Figure 12 Distribution of gullies in the southern hemisphere. Due to the challenges of resolving km-scale features at the global scale, nearby features were aggregated. Gullies are displayed according to the type of feature upon which they formed. The survey ranged from 20° to 90°S.

of Martian history. There are some gullies found on the inside of crater rims in this region as well, suggesting that there is nothing intrinsic about the valley itself that would lead to gully formation, just that it provides steep slopes that are required for gully formation.

Gullies are, by a considerable margin, most common between 30° and 45°S: 10,747 of the 14,719 gullies (73.0%) mapped as part of this survey are within this latitude band. While this is in part due to there being more physical terrain at higher latitudes, the map of gully distribution (Figure 12) shows that this in insufficient to explain the paucity of gullies broadly at higher latitudes. This is consistent with previous analyses that have argued that the lack of steep slopes at these latitudes (Kreslavsky and Head, 1999) inhibits gully formation on the softened terrain that dominates the high- latitudes of Mars (Dickson and Head, 2009). Another possible explanation, however, is that it rarely gets

warm enough to melt ice at the surface in the polar regions of Mars. This will be tested with this geodatabase below when the LMD-GCM simulations is used to predict the temperatures that should be experienced at these latitudes.

Gullies on crater rims (both full and insufficient) and valley walls follow the same trend by being most common between 30-45°S. Gullies on mesas, however, have a broader latitudinal range (Figure 12). When mapped (Figure 12), they are most common around the Argyre impact basin. This could be due to: (1) a greater concentration of this type of host feature in this region; and/or (2) climate conditions dictated by the basin itself, since its low elevation may be more conducive to the presence of liquid water because of increased pressure. This can be tested with GCMs.

Gullies on dune faces are almost entirely located within the 40-55°S latitude band. From the distribution map (Figure 12), they are mostly found within a few specific dune fields between 20 and 40°E. Most likely, this is due more to the location of dune fields than anything unusual about the gully forming process.

Finally, gullies in polar pits are, as expected, only found at very high latitudes (Figures 12-13). These gullies provide an end-member for analysis with the LMD-GCMs, as they may be outside of the range of where temperatures can surpass the melting point on Mars. This is a scenario in which gully distribution is completely controlled by the distribution of the host feature. Crater rims, on the other hand, provide a more random distribution of surface features, though craters are more heavily degraded at higher latitudes on Mars. Thus, it is still beneficial to integrate gullies on all surface types to truly characterize their distribution.
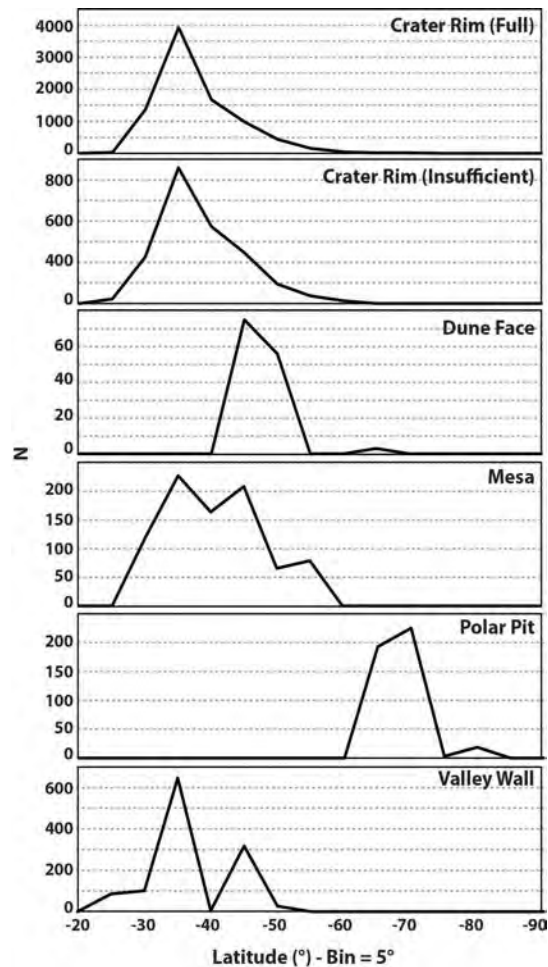
Figure 13 Gullies as a function of latitude. Note the varying scales on the y-axis. Gullies are most common in the mid-latitudes of the southern hemisphere, with 73% forming between 30°S and 45°S. Dunes, mesas and polar pits appear to be controlled more by the localized availability of those types of features as opposed to something intrinsic to the gully forming process.

4.1.2 Gully distribution as a function of elevation

The 0 m vertical datum of Mars has been arbitrarily set at the elevation where atmospheric pressure at the surface corresponds to the triple point of water (the temperature/pressure conditions where water could be a solid, liquid or gas) under
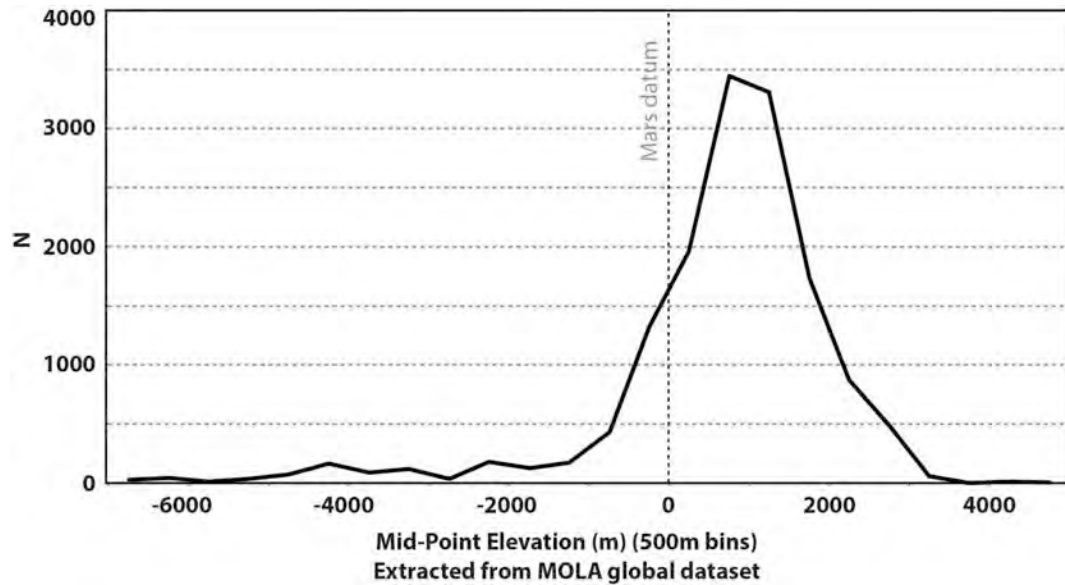
Figure 14 Gullies as a function of elevation. Gullies form from ~-6 km to ~4km above the datum. Approximately 81.5% of gullies form above the datum, which is where conditions are below the triple point of water on present-day Mars.

present conditions. Thus, elevations below the datum could potentially permit liquid water at the surface today, while elevations above the datum are unlikely to do so.

Altimetry values were extracted from the Mars Orbiter Laser Altimeter global DEM of Mars at gully locations (463 m/px), yielding a histogram of gully elevations (Figure 14). Gullies occur at a wide range of elevations, from -6,948m below the datum to 4,611m above. Gullies are preferentially above the datum, between 0 and 2,000 m: 12,003 of the 14,719 gullies mapped (81.5%) are above the datum, where liquid water should be unstable under present-day conditions due to insufficient surface pressure. This provides compelling evidence that if gullies are forming today in these locations, liquid water is an unlikely source for their erosion.
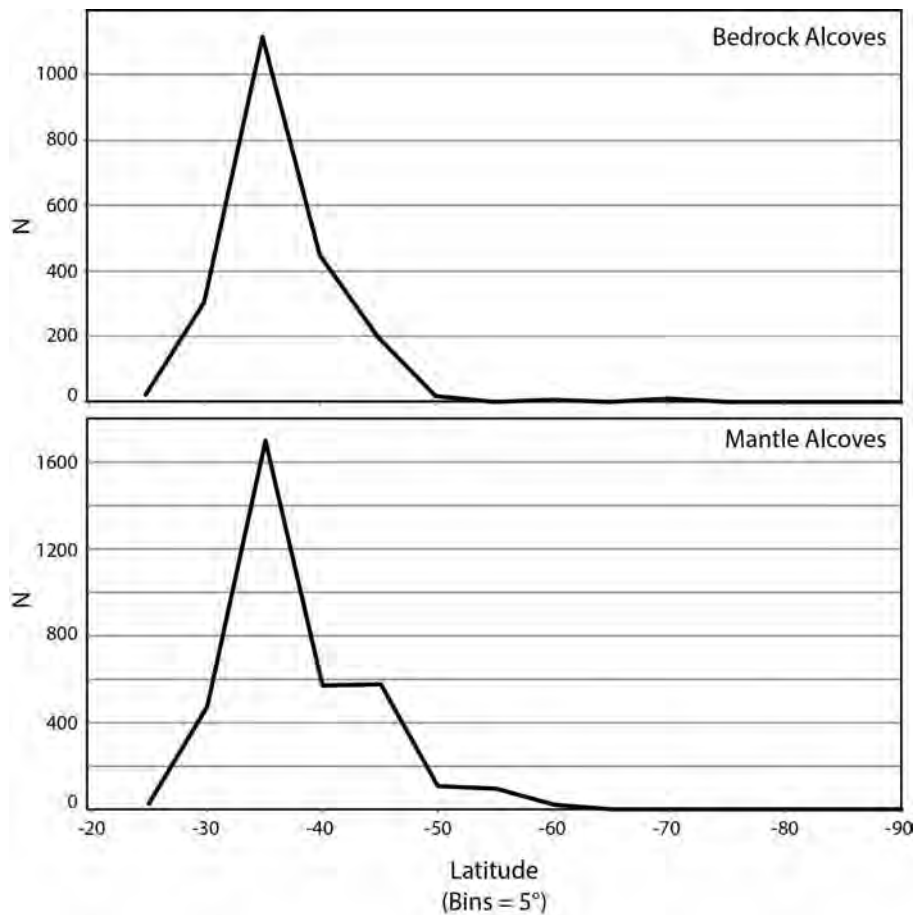
Figure 15 Latitude distribution by alcove type. Alcoves within the LDM are more common at slightly higher latitudes than bedrock alcoves, which is consistent with the LDM being a hemisphere-wide mantling unit that is more pervasive at higher latitudes (Head et al., 2003).

4.1.3 Gully distribution as a function of alcove type

Of the 14,719 gullies that were mapped, 2,140 were determined to have formed with bedrock alcoves while 3,613 were determined to have formed entirely within the LDM. Each type forms most commonly in the 30-40°S latitude band (Figure 15), though alcoves eroded into the LDM are slightly more common at higher latitudes. Since the LDM is thought to drape much of the terrain on Mars at higher latitudes in each

hemisphere (Head et al., 2003), one would expect this relationship, as exposed bedrock becomes less and less common at higher latitudes.

4.1.4 Gully distribution as a function of orientation

Numerous studies have attempted to determine whether or not gullies form on preferred slope orientations on Mars (Malin and Edgett, 2000; Costard et al., 2002; Heldmann and Mellon, 2004; Berman et al., 2005; Balme et al., 2006; Bridges and Lackner, 2006; Dickson, Head, and Kreslavsky, 2007; Heldmann et al., 2007; Kneissl et al., 2010). Only one of these studies (Berman et al., 2005) filtered their catalog of gullies to only include craters that provide 360° of slope orientation, but this was a regional study that was performed before CTX data were available. With the geodatabase created in this study and the coded domains that were built in, this measurement can be made across the entire southern hemisphere.

In total, 8,704 gullies were mapped as forming on "Crater Rim (full)," which provides sufficient statistics for deciphering trends. When plotted as a function of latitude (Figure 16), gullies are almost exclusively poleward facing in the 25-40°S latitude band. This is consistent with previous studies that measured orientation from other datasets at this latitude (Heldmann and Mellon, 2004; Balme et al., 2006; Dickson, Head, and Kreslavsky, 2007). At higher latitudes (40-55°S), more equator-facing gullies are found. Previous surveys had indicated that gullies in this latitude band were mostly equator-facing (Heldmann and Mellon, 2004). These results show a more balanced distribution. Locations poleward of 55°S provide insufficient statistics for evaluating orientation preferences, though a possible return to pole-ward facing gullies
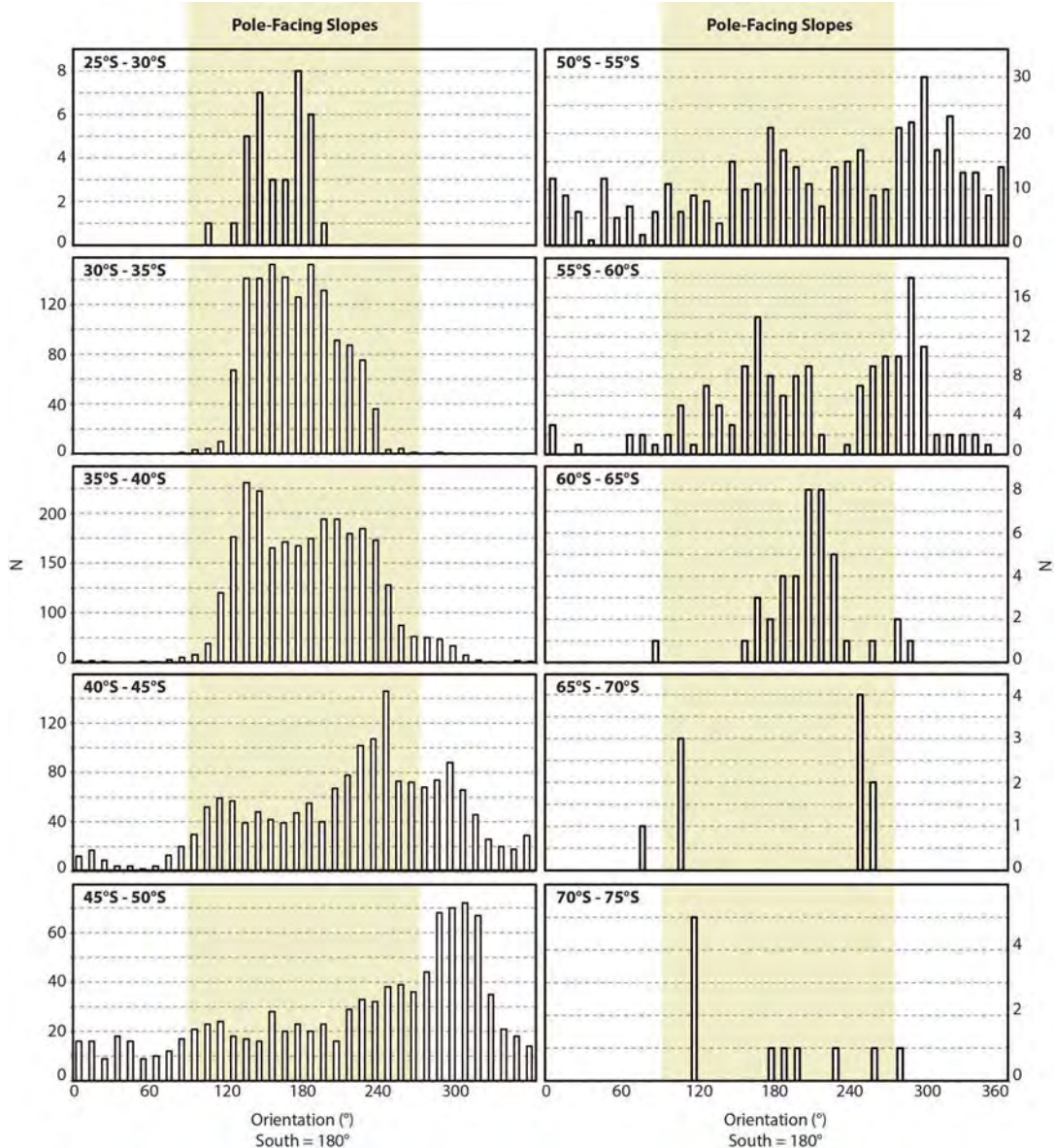
Figure 16 Orientation as a function of latitude. Gullies are exclusively pole-facing at mid-latitudes and equally distributed at higher latitudes. This may have more to do with where ice can accumulate as opposed to where it can melt.

may be revealing itself through the data. The lack of fresh impact craters at these polar latitudes makes this measurement extremely difficult.

The poleward preference for gullies in the mid-latitudes is counter-intuitive, since these are the colder walls of an impact crater. It is thought that this is possibly due to these locations being more conducive to ice-accumulation (Hecht, 2002). The LMD-

45

GCMs used in this study are unable to resolve slopes at this scale and work under the assumption that there is already ice on the ground to be melted. Thus, this question cannot be tested with the data presented here but is a natural follow-up investigation using similar analysis techniques.

4.2 Liquid water stability at gully locations

The geodatabase of gullies in the southern hemisphere of Mars was integrated with GCM simulations in two ways: (1) generation of animations of temperature/pressure conditions with gullies mapped on the same map; and (2) extraction of data from gully sites to track a conditional query: how many times during each simulation does each gully site experience conditions that would allow for the melting of H_2O ice?

The results of both of these techniques are now presented so as to provide a first order assessment of what this says about the potential of liquid water on the surface of recent Mars.

4.2.1 Qualitative assessment of liquid water stability

The pipeline described in Section 3.3.1 produced three separate animations, all with 5,352 frames that correspond to the number of time steps in each of the three GCM simulation runs (Appendix C). Each frame represents surface conditions for 1/8 of a martian day. These animations are all provided as supplemental material to this manuscript (Video 1, Video 2 and Video 3, corresponding to simulation runs at obliquity values of 25°, 30° and 35°). For static representations, frames have been extracted and shown in Figures 17 and 18. Figure 17 shows an 8-frame sequence that illustrates diurnal
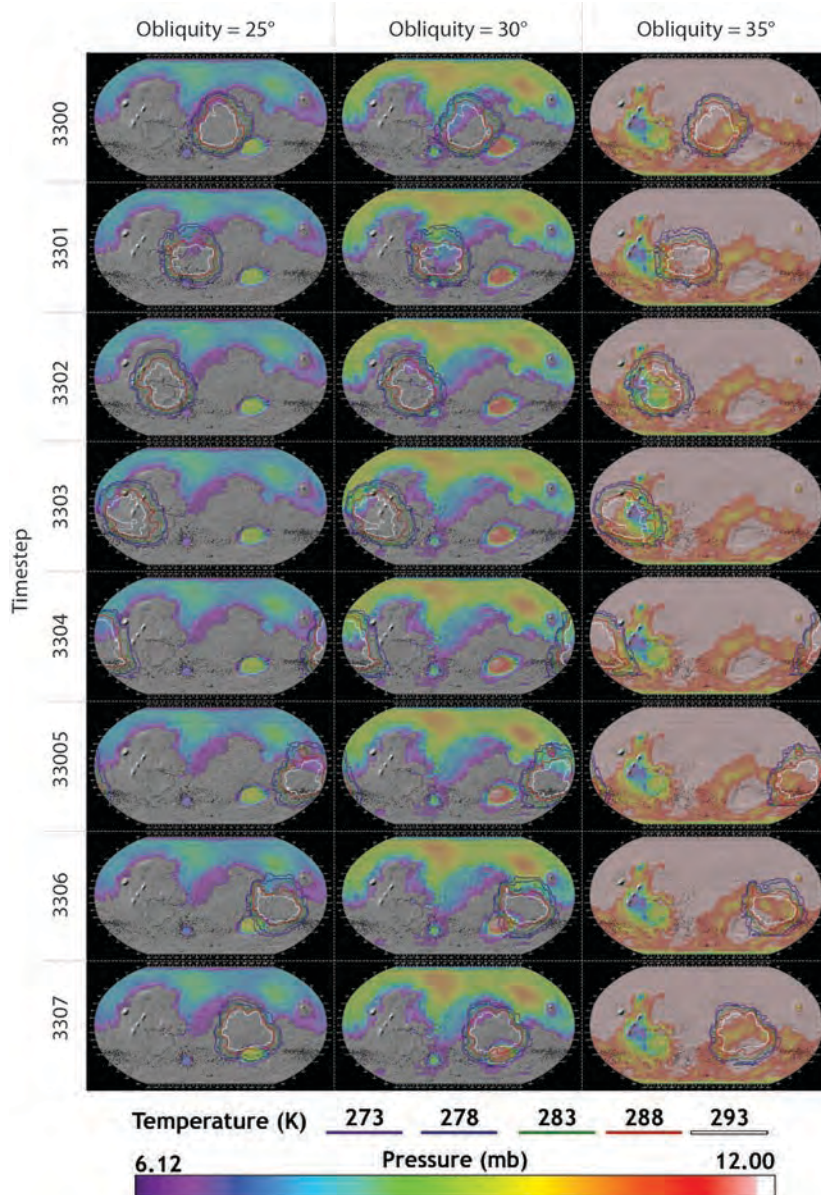
Figure 17   GCM time steps over one martian day. Samples from Video 1 (obliquity = 25°), Video 2 (30°) and Video 3 (35°). Each vertical strip represents one martian day. Regions where liquid water could exist are areas where a pressure value is displayed and falls within the temperature contours. Gullies are mapped in black.

conditions over the course of one martian day for each scenario. Time steps 3300-3307

correspond to spring in the southern hemisphere. Figure 18 shows each model run in

different seasons, to get a sense of the annual cycle on Mars. To facilitate comparisons

between model runs, the same color ramps and scales were used for tracking pressure
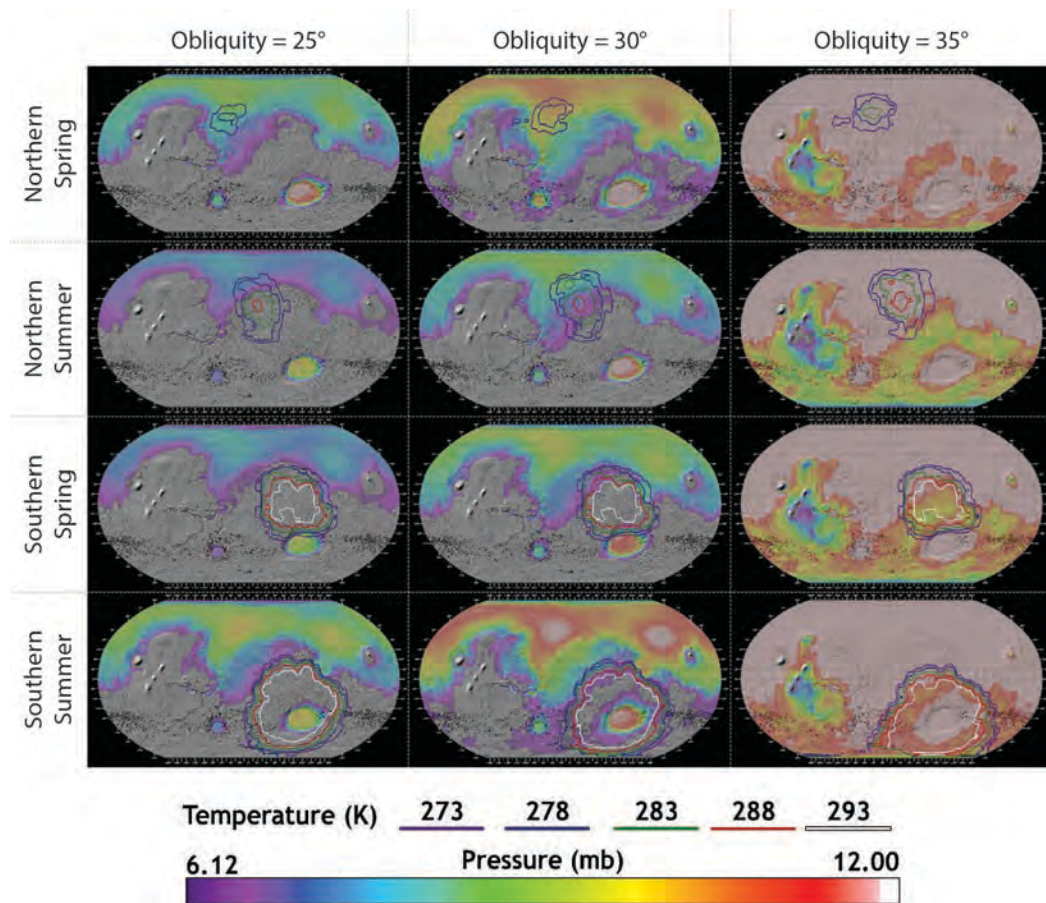
Figure 18 GCM time steps over one martian year. Samples from Video 1 (obliquity = 25°), Video 2 (30°) and Video 3 (35°). Each vertical strip represents a year on Mars. Regions where liquid water could exist are areas where a pressure value is displayed and falls within the temperature contours. Gullies are mapped in black.

(raster) and temperature (contour). Any values that are below the triple point of water (T

< 273 K or P < 6.11 mb) were represented as null values. Therefore, regions that display

a pressure value and fall within the contour bands are above the triple point of water.

In the 25° scenario (Video 1, Figures 17 and 18), very few of the gullies that were

mapped occur in regions where the pressure is sufficient to allow for liquid water at the

surface. Exceptions to this are on the floors and along the margins of the major impact

basins, Argyre and Hellas. Temperature conditions, however, surpass the melting point

at almost all locations during southern summer (Figures 18 and 19). The LMD-GCM
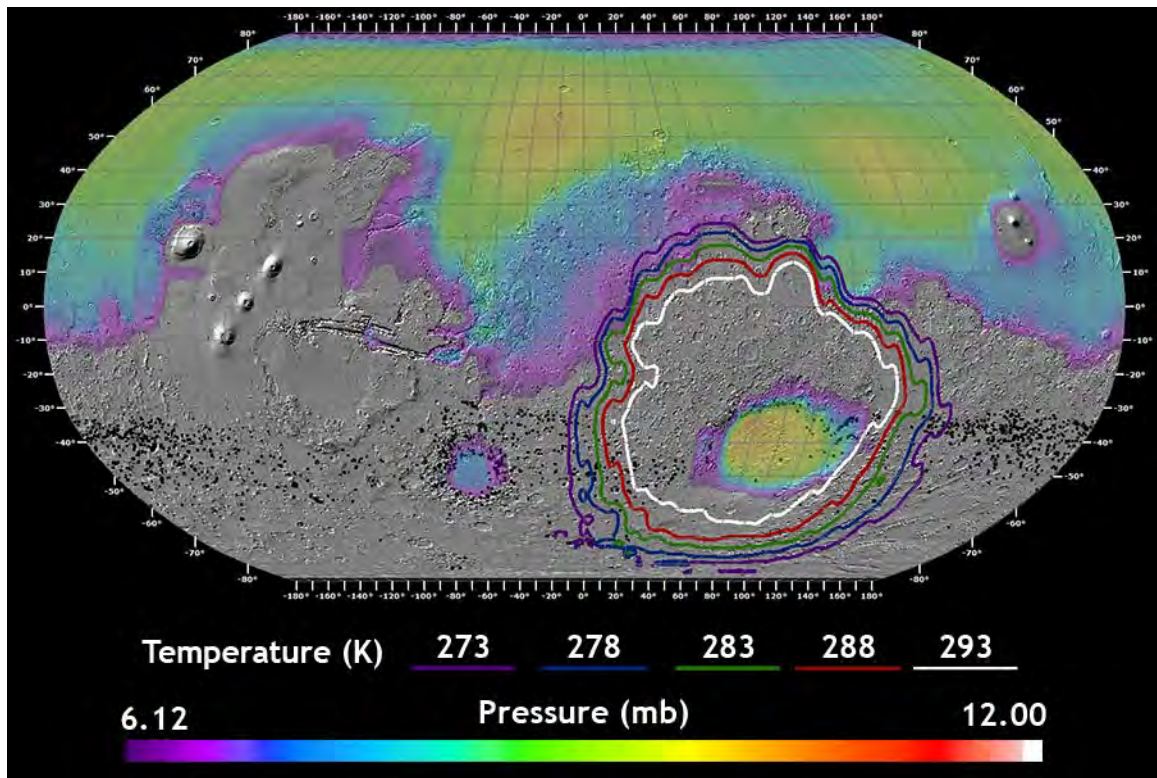
Figure 19 GCM/data rendering of southern summer, 25° obliquity. One time step from Southern summer under 25° obliquity conditions. Mid-day temperatures surpass the melting point of H$_2$O (273 K) at almost all latitudes of the southern hemisphere. Surface pressures, however, only surpass the triple point (6.11 mb) around major impact basins. Gullies are mapped in black.

results reflect the phenomenon that due to the highly elliptical orbit of Mars, summer in the southern hemisphere is considerably warmer than summer in the northern hemisphere. This is less obvious from the quantitative results discussed below. Quantitative techniques, at least the ones presented here, are unable to provide context in the same way as the qualitative techniques.

When the obliquity is set to 30° (Video 2, Figures 18 and 20), which is a scenario that Mars encountered ~380,000 years ago (Laskar, Levrard, and Mustard, 2002), conditions slightly improve in the southern hemisphere for liquid water stability, but still
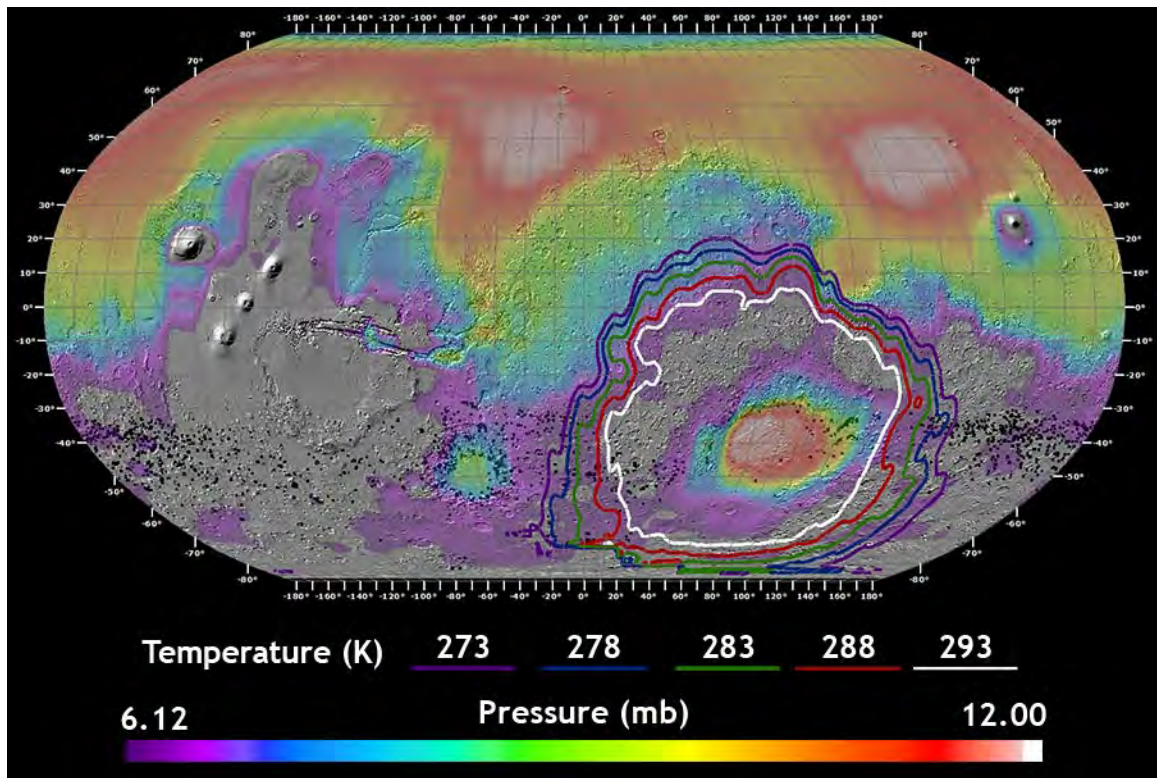
Figure 20 GCM/data rendering of southern summer, 30° obliquity. One time step from Southern summer under 30° obliquity conditions. Surface pressures surpass the triple point (6.11 mb) across a greater percentage of the southern hemisphere, but not over many gully locations. Gullies are mapped in black.

most regions in the southern highlands that contain gullies fall below the triple point of water in terms of surface pressure. During the northern summer, the planet is further away from the sun, so CO_2 and H_2O are mostly at the poles, trapped as ice. During the southern summer, when the planet is much closer to the sun, more of that ice is sublimated into the atmosphere, increasing surface pressure across the planet and expanding the zone of liquid water stability.

The final scenario, with the obliquity set to 35° (Video 3, Figures 18 and 21), which occurred ~625,000 years ago (Laskar, Levrard, and Mustard, 2002), reveals a planet where liquid water could potentially exist almost anywhere. Only the Tharsis
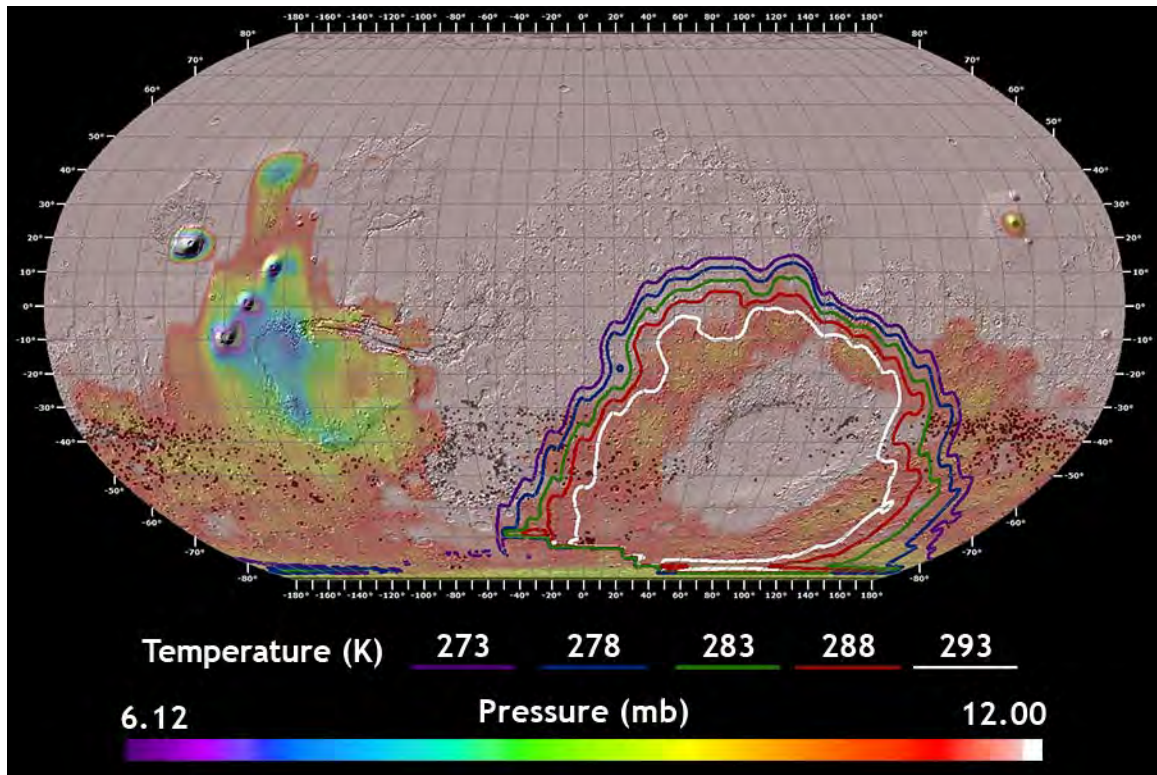
Figure 21 GCM/data rendering of southern summer, 35° obliquity. One time step from Southern summer under 35° obliquity conditions. Surface pressures surpass the triple point (6.11 mb) across the entire southern hemisphere, over every mapped gully location. Gullies are mapped in black. Under these conditions, liquid water could potentially exist at all locations in the southern hemisphere.

volcanoes maintain conditions where surface pressure is too low to ever permit liquid water at the surface. In the southern hemisphere where gullies are found, every gully site occurs in a location where the pressure at the surface is greater than 6.11 mb every day of the year. Thus, liquid water stability is no longer a function of surface pressure, but of temperature. As can be seen in Figures 17 and 18, when compared to the other simulations, surface temperature does not increase dramatically.
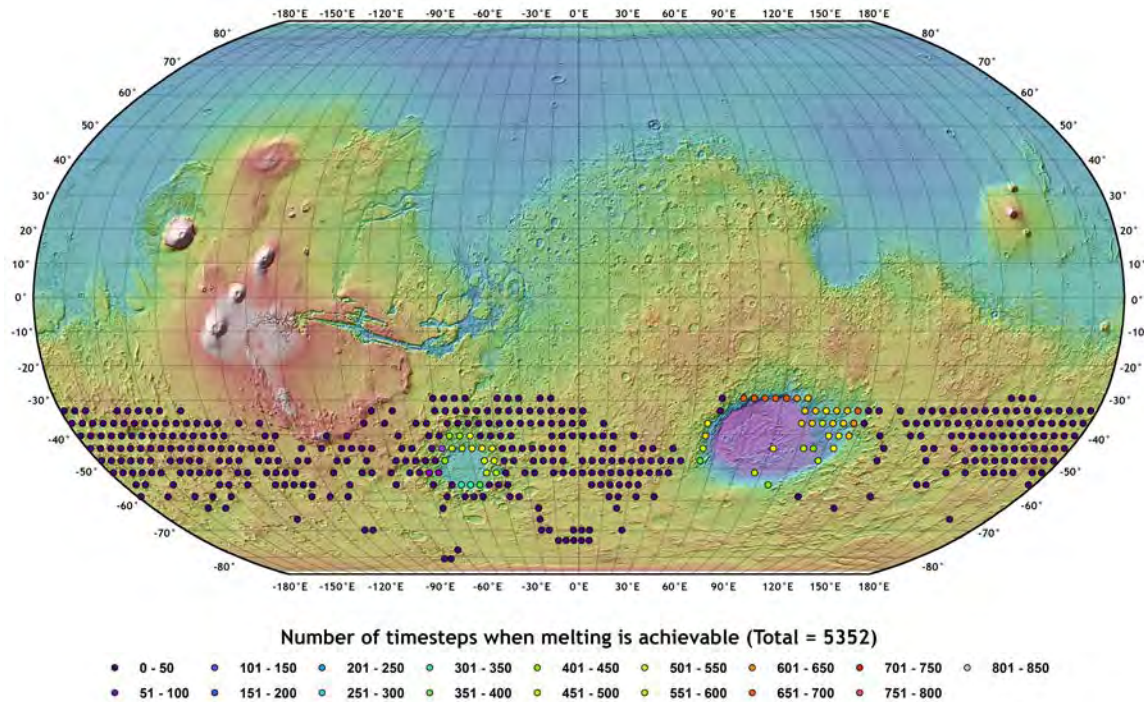
**Figure 22 Integration of GCM simulations and the gully geodatabase under 25°
obliquity (present-day). Each point represents the center of a cell in the GCM
simulation that overlapped at least one gully. Regions between 20°S and 90°S
without points had no gullies mapped. In this scenario, melting was only
achievable along the margins and on the floors of the major impact basins
Argyre (left) and Hellas (right).**

4.2.2 Quantitative assessment of liquid water stability

For each gully site on Mars, time steps when surface conditions surpassed the triple point
of water at that site were counted separately for each simulation. Thus, if gully site x
experienced temperature $> 273^o$ K and pressure > 6.11 mb during a time step, that time
step was tallied. This final number after iterating through all 5,352 time steps was logged
as N (number of time steps when melting was achievable). One possible caveat specific
to this instance is that should conditions on the surface become too warm, water on the
surface will boil and return to a vapor state. However, the temperature needs to reach
273 K first before it reaches the boiling point. Thus, this method does not discern exactly
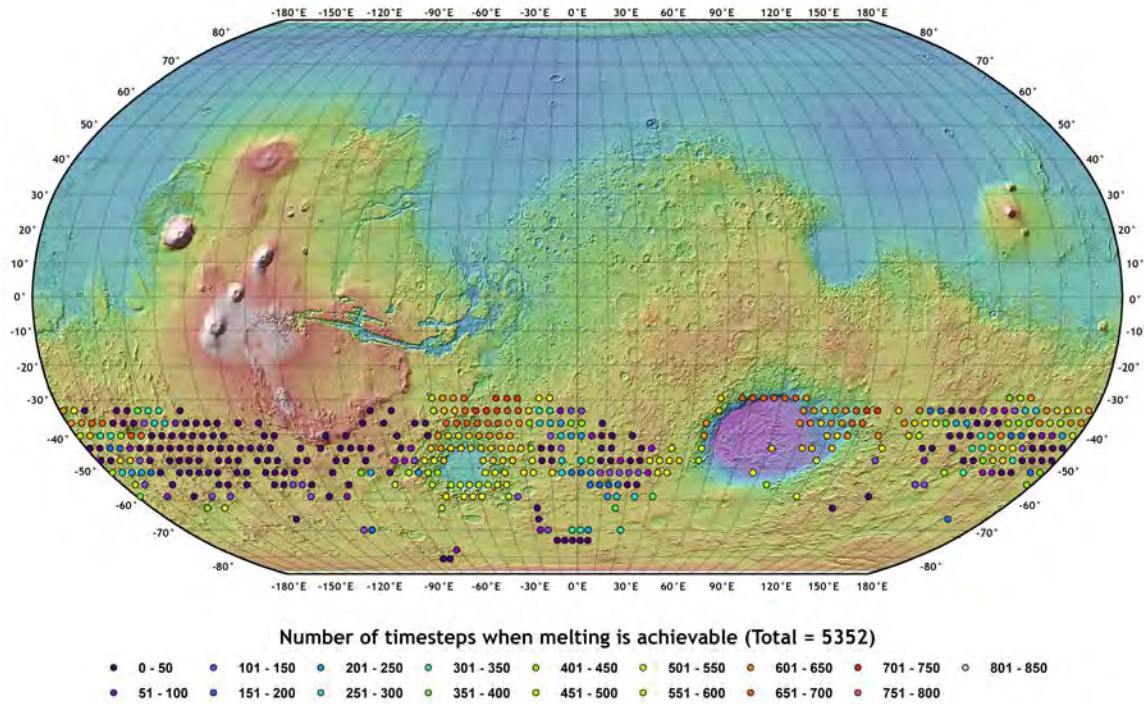
Figure 23 GCM integration under 30° obliquity simulation. Each point represents the center of a cell in the GCM simulation that overlapped at least one gully. Regions between 20°S and 90°S without points had no gullies mapped. In this scenario, melting could occur in many regions of the southern highlands, but it is insufficient to explain all gullies.

how long the liquid water could have remained on the surface, only that conditions were sufficient to change its phase to liquid in the first place.

As the qualitative video suggests (Video 1), very few gully sites in the southern hemisphere achieved melting conditions during the 25° simulation, which reflects conditions on the surface of Mars today (Figure 22). The only sites that achieved conditions above the triple point are those on the rims and floors of the giant impact basins Argyre and Hellas, where low elevations provide increased surface pressures.

When the integration pipeline is conducted with the 30° obliquity scenario (Figure 23), a wider swath of the southern highlands becomes conducive to liquid water at the surface. Again, both major impact basins are foci for liquid water stability, and
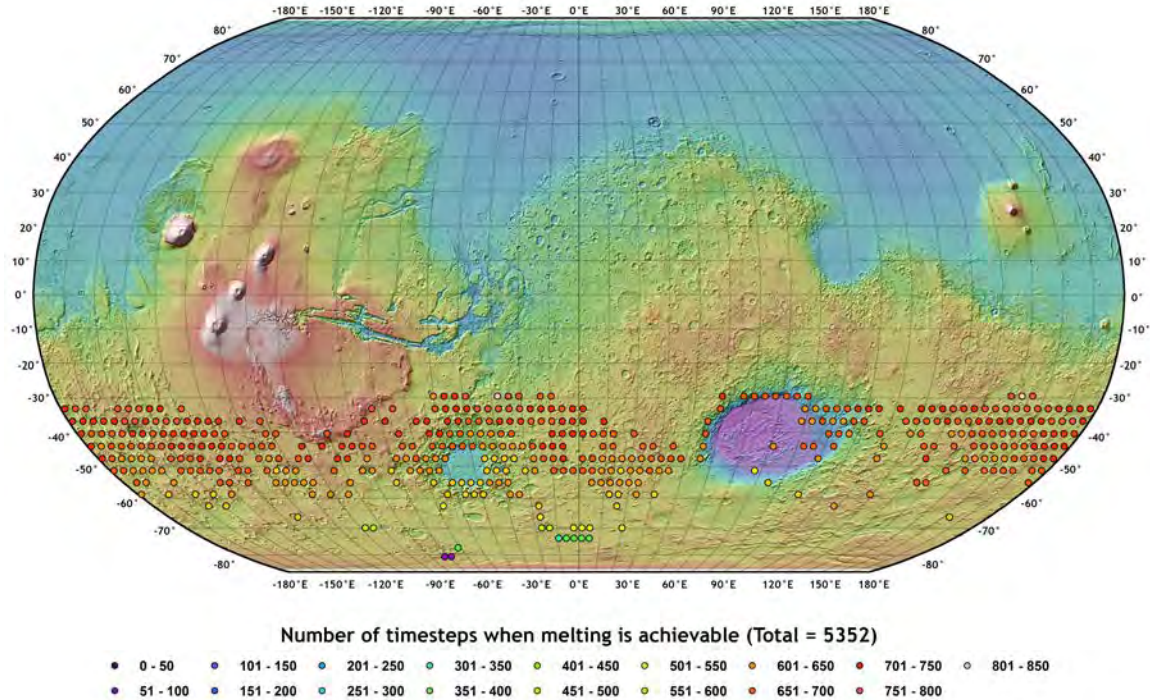
Figure 24   GCM integration under 35° obliquity simulation. Each point represents the center of a cell in the GCM simulation that overlapped at least one gully. Regions between 20°S and 90°S without points had no gullies mapped. In this scenario, melting conditions were achieved at every location where gullies were mapped in the geodatabase.

patchy regions of the mid-latitudes see some periods of time under potential melting conditions.   That said, there are still large regions with large populations of gullies that never see conditions when ice on the surface of the planet would melt instead of sublimate. This map nicely demonstrates that melting of ice on Mars under this scenario is not a function of latitude, but of elevation due to its extremely thin atmosphere. If gullies are indeed formed by liquid water, conditions represented by this scenario are insufficient to account for them at all locations.

Finally, the leap from 30° to 35° obliquity (Figure 24) surpasses the threshold at which all gullies on Mars can be explained by the presence of liquid water. Every site experiences at least 67 time steps (the equivalent of ~8 martian days) above the triple

point of water. Unlike the 30° simulation, this run shows that melting is controlled almost entirely by latitude, such that lower-latitude sites experience more time steps above the melting point than higher-latitude sites. Integrating GCMs and data in this way allows discriminating when melting on Mars is limited by temperature and when it is limited by pressure.

Taken together, the qualitative and quantitative analyses from this project suggest the following:

(1) Gully activity observed today (Malin et al., 2006; Diniega et al., 2010; Reiss et al., 2010; Dundas et al., 2012) is unlikely to be caused by the melting of water at the surface unless it is in the vicinity of a major impact basin and occurs in southern summer; and

(2) Conditions under 35° obliquity are so favorable to liquid water existing (for up to ~100 cumulative days in some locations) that this model may over-predict where liquid water could be. This may be due to the assumption that during 35° obliquity conditions, average atmospheric pressure is ~10 mb (Phillips et al., 2011), which may be an over-estimate.

CHAPTER FIVE: CONCLUSIONS

The ongoing effort to document liquid water on Mars focuses on several major questions, three of which are: (1) Where has water existed as a liquid?; (2) How much was there?; and (3) How long was it there? Since these questions are being addressed almost entirely with remote sensing data, the answers can only be approached from the confluence of multiple data sets collected by multiple highly specialized investigators and instruments. GIS represents the best available environment for spatial data integration, extraction, and visualization.

Based upon the integration analysis in this study, melting of ice at or near the surface today could only potentially happen for very brief periods of time on the floors and along the rims of the Argyre and Hellas impact basins, which provide the lowest topography in the hemisphere. This is consistent with the only other published attempt to map regions on present-day Mars where liquid water can exist (Haberle et al., 2001) (Figure 7), which used the AMES-GCM. It is also consistent with recent observations of contemporary activity within pre-existing gullies, which occur in regions and at times in the martian year when liquid water should not be present (Diniega et al., 2010; Dundas et al., 2012).

Given our current understanding of Mars within the last several million years, conditions for melting peaked most recently ~625,000 years ago (Laskar, Levrard, and Mustard, 2002), when the rotational axis was tilted 10° more than it is today. This made CO_2 at the polar caps unstable, sublimating large reservoirs of CO_2 ice into the atmosphere (Phillips et al., 2011), and increasing pressure across the entire planet to ~10

mb. If the assumptions of the models used in this study are accurate, liquid water is possible at all 14,719 locations where gullies have been mapped in the presented geodatabase. Qualitative (Figures 17-18) and Quantitative (Figures 22-24) analyses reveal a transition in the stability regime of liquid water on the surface of Mars as a function of obliquity:

(1) Low Obliquity (25°): Regions for liquid water are controlled primarily by elevation (Figure 14), as the majority of gullies occur in locations where pressure does not surpass the triple point; and

(2) High Obliquity (35°): Regions for liquid water are controlled primarily by latitude, such that gullies are more likely to form in the warmer mid-latitudes than the colder high-latitudes.

The surface of Mars exhibits many features that show strong latitude dependence (Head et al., 2003; Milliken, Mustard, and Goldsby, 2003), and understanding how different latitudes of Mars behave in different ways under different orbital conditions could help further the understanding of water and ice-related phenomena.

While informative, this technique only accounts for one half of the story. Achieving conditions for melting is only interesting if there is ice at or near the surface to melt. The GCM integration approach documented here could potentially provide the missing link to decipher the end-to-end water cycle during the most recent history of Mars. For instance, several lines of evidence, including morphological data (Head et al., 2003; Mustard, Cooper, and Rifkin, 2001), spectral evidence (Vincendon et al., 2010), recent impact exposures (Byrne et al., 2009), gamma-ray/neutron data (Boynton et al., 2002; Feldman et al., 2002), and lander analysis (Smith et al., 2009) point to the mid-

latitudes of Mars containing high volumes of H_2O ice within the top meter of the surface. Deciphering how and when it got there is critical for understanding whether it was in place during periods when melting was more likely than it is today (Figure 24, Video 3).

Recent modeling using the LMD-GCM has shown that under 35° obliquity conditions, accumulation of an ice-rich surface layer is predicted in the mid-latitudes (Madeleine et al., 2013), broadly where near-surface ice is thought to occur. Integrating these GCM simulations with surface mapping of the suite of ice-related features in a geodatabase framework will allow for a more thorough understanding of not just what happens to ice on Mars, but how it gets there in the first place. If both of these findings are true, then the results could be that Mars undergoes optimal periods when both the accumulation of ice on the surface and the melting of that ice are simultaneously optimized.

This approach also has potential for answering questions about early Mars, when water was more abundant across the surface (Carr, 1996). The astronomical understanding of Mars' orbital properties are not as well constrained for this period of history (Laskar et al., 2004), but progress is still being made to produce GCMs that provide boundaries for what the early Mars climate may have been like. Unlike present-day conditions, however, when gullies provide the primary evidence for fluvial erosion, early Mars exhibits a wide range of features that point to large volumes of water at or near the surface, including valley networks (Hynek, Beach, and Hoke, 2010), open basin lakes (Fassett and Head, 2008), hydrated mineralogy using hyperspectral orbital imaging (Bibring et al., 2006), also confirmed by in-situ chemical analysis (Squyres et al., 2004). The diversity in surface features amplifies the importance of using a geodatabase

architecture that can accommodate this range of features, as perhaps not all features formed at the same time or by the same means.

5.1 Future Work

The technique developed in this study can also be used to investigate other processes besides the stability of potentially fluid substances on the martian surface. For instance, properly modeling wind behavior is valuable not only for scientific analysis but also for engineering considerations: landing spacecraft on another planet requires detailed information regarding the wind regimes in various regions to protect the spacecraft during entry, descent and landing. Recent studies have used different methods for registering surface features with wind models derived from GCMs. First, dune orientations contain information about dominant wind directions and potentially about wind strength. Preliminary studies have attempted to correlate these observations with GCM predictions (Hayward et al., 2009). Second, ash dispersal from eruptions of volcanoes on Mars is controlled by the density of the atmosphere and wind speed/direction. Modeling of this process has led to correlations with enigmatic surface features found in the tropics of Mars (Kerber et al., 2012). Both of these projects are ideal for GCM/database integration to help further the understanding of eolian dynamics in low-density atmospheres.

The computational processes described in this study are also scale-independent. Climate model outputs that are not global in nature could be incorporated into the pipeline described here, which would provide valuable high-resolution information about stability conditions as a function of local topography. For instance, the pole-facing wall

of a crater experiences a different temperature cycle than the equator-facing wall in the mid-latitudes where gullies form. This disparity cannot be resolved with current models when integrating over the entire planet, but mesoscale models that focus on specific areas (Bertrand et al., 2013) would provide this type of high-resolution analysis of specific targets.

GCM/data integration is not limited by planet or input dataset. In terrestrial geoscience studies there is a wide use of netCDF among the climatology, environmental and oceanography communities. Software specifically suited to processing multi-dimensional datasets are likely to be of value for optimizing throughput when integrating these data with surface mapping datasets. Open source tools outside the ArcGIS environment, such as Basemap Matplotlib Toolkit 1.0.8 (Matplotlib Basemap Toolkit, 2014), may provide more tailored functionality to maximize the information that is extracted from these high-volume data sets. Other tools from the Open Geospatial Consortium (OGC) encompass a suite of open standards for inter-community data exchange, some involving netCDF. These technologies might be considered in future work and integration, using the pipeline described in this study to bridge between open source approaches and ArcGIS.

The tools developed as a part of this project are designed to be as versatile as possible. Thus, models that try to replicate ancient climates on the Earth can be incorporated. What was the Earth's climate like when turtles and alligators thrived at 80°N in the Early Eocene (~50Ma ago) (Estes and Hutchison, 1980)? How much different is that from projections of the Earth's climate over the next century? Accurate geodatabases of paleoclimate indicators like climate-sensitive biota can be used for

integration with sophisticated GCMs of the Earth at these times. Helping to make the GCMs more robust is essential for producing accurate forecasts of the implications of contemporary greenhouse warming over the next century.

This proof-of-concept study of gullies on Mars serves as a demonstration of what GIS is capable of revealing when provided with high-volume, diverse and flexible data sets from GCM simulations. Each data set has value on its own, but their full potential can only be realized when integrated together and analyzed in concert.

REFERENCES

Akinyemi, F., and J. Adejuwon. 2008. A GIS‑Based Procedure for Downscaling Climate Data for West Africa. *Transactions in GIS* 12 (5): 613-631.

Albrecht, J. 1996. Universal GIS operations for environmental modeling. Proc. 3rd International Conference/Workshop on Integrating GIS and Environmental Modeling.

Andrews-Hanna, J., M. Zuber, and W. Banerdt. 2008. The Borealis basin and the origin of the martian crustal dichotomy. *Nature* 453: 1212-1215.

Balme, M., N. Mangold, D. Baratoux, F. Costard, M. Gosselin, P. Masson, P. Pinet, and G. Neukum. 2006. Orientation and distribution of recent gullies in the southern hemisphere of Mars: Observations from High Resolution Stereo Camera/Mars Express (HRSC/MEX) and Mars Orbiter Camera/Mars Global Surveyor (MOC/MGS) data. *Journal of Geophysical Research (Planets)* 111: 05001.

Berman, D., W. Hartmann, D. Crown, and V. Baker. 2005. The role of arcuate ridges and gullies in the degradation of craters in the Newton Basin region of Mars. *Icarus* 178: 465-486.

Bertrand, T., A. Spiga, S. Rafkin, A. Colaitis, F. Forget, and E. Millour. 2013. LMD - SwRI Martian Mesoscale Models Intercomparison for ExoMars Landing Site Characterization. *European Planetary Science Congress 2013, held 8-13 September in London, UK.*

Bibring, J-P., Y. Langevin, J. Mustard, F. Poulet, R. Arvidson, A. Gendrin, B. Gondet, N. Mangold, P. Pinet, and F. Forget. 2006. Global Mineralogical and Aqueous Mars History Derived from OMEGA/Mars Express Data. *Science* 312:400-404.

Bivand, R., and A. Lucas. 2000. Integrating models and geographical information systems. In *Geocomputation*, ed. S. Openshaw and R. Abrahart, 340-373. London: Taylor & Francis.

Boynton, W., W. Feldman, S. Squyres, T. Prettyman, J. Bruckner, L. Evans, R. Reedy, R. Starr, J. Arnold, D. Drake, P. Englert, A. Metzger, I. Mitrofanov, J. Trombka, C. d'Uston, H. Wanke, O. Gasnault, D. Hamara, D. Janes, R. Marcialis, S. Maurice, I. Mikheeva, G. Taylor, R. Tokar, and C. Shinohara. 2002. Distribution of Hydrogen in the Near Surface of Mars: Evidence for Subsurface Ice Deposits. *Science* 297: 81-85.

Bridges, N., and C. Lackner. 2006. Northern hemisphere Martian gullies and mantled terrain: Implications for near-surface water migration in Mars' recent past. *Journal of Geophysical Research (Planets)* 111: 09014.

Buckley, A. 2013. Using Valid Value Tables in Geodatabase Design to Define Feature Types. *Cartographic Perspectives* (48): 57-61.

Byrne, S., C. Dundas, M. Kennedy, M. Mellon, A. McEwen, S. Cull, I. Daubar, D. Shean, K. Seelos, S. Murchie, B. Cantor, R. Arvidson, K. Edgett, A. Reufer, N. Thomas, T. Harrison, L. Posiolova, and F. Seelos. 2009. Distribution of Mid-Latitude Ground Ice on Mars from New Impact Craters. *Science* 325: 1674-1676.

Carr, M. 1996. *Water on Mars*. New York, USA: Oxford Univ. Press.

Childs, C. 2009. The Top Nine Reasons to Use a File Geodatabase. *ArcUser* (Spring 2009): 12-15.

Christensen, P. 2000. Introduction to the special section: Mars Global Surveyor Thermal Emission Spectrometer. *Journal of Geophysical Research* 105: 9507-9508.

Christensen, P., B. Jakosky, H. Kieffer, M. Malin, H. McSween, Jr., K. Nealson, G. Mehall, S. Silverman, S. Ferry, M. Caplinger, and M. Ravine. 2004. The Thermal Emission Imaging System (THEMIS) for the Mars 2001 Odyssey Mission. *Space Science Reviews* 110: 85-130.

Costard, F., F. Forget, N. Mangold, and J. Peulvast. 2002. Formation of Recent Martian Debris Flows by Melting of Near-Surface Ground Ice at High Obliquity. *Science* 295: 110-113.

Dickson, J., and J. Head. 2009. The formation and evolution of youthful gullies on Mars: Gullies as the late-stage phase of Mars' most recent ice age. *Icarus* 204: 63-86.

Dickson, J., J. Head, and L. Barbieri. 2013. Martian Gullies as Stratigraphic Markers for Latitude-Dependent Mantle Emplacement and Removal. *Lunar and Planetary Science Conference* 44: 1012.

Dickson, J., J. Head, and M. Kreslavsky. 2007. Martian gullies in the southern mid-latitudes of Mars: Evidence for climate-controlled formation of young fluvial features based upon local and global topography. *Icarus* 188: 315-323.

Diniega, S., S. Byrne, N. Bridges, C. Dundas, and A. McEwen. 2010. Seasonality of present-day Martian dune-gully activity. *Geology* 38 (11): 1047-1050.

Dundas, C., S. Diniega, C. Hansen, S. Byrne, and A. McEwen. 2012. Seasonal activity and morphological changes in martian gullies. *Icarus* 220: 124-143.

Esri. 2007. What's New in ArcGIS 9.2. http://webhelp.esri.com/arcgisdesktop/9.2/pdf/whats_new_in_arcgis_92.pdf (last accessed 28 April 2014).

Esri. 2014a. What's New in ArcGIS 10.2.x.. http://resources.arcgis.com/en/help/pdf/whats_new_in_arcgis.pdf (last accessed 28 April 2014).

Esri. 2014b. Working with NetCDF Data in ArcGIS 10.1. http://training.esri.com/gateway/index.cfm?fa=catalog.webCourseDetail&courseID=2568 (last accessed 23 April 2014).

Estes, R., and J. Hutchison. 1980. Eocene lower vertebrates from Ellesmere Island, Canadian Arctic Archipelago. *Palaeogeography, Palaeoclimatology, Palaeoecology* 30: 325-347.

Fassett, C., and J. Head. 2008. Valley network-fed, open-basin lakes on Mars: Distribution and implications for Noachian surface and subsurface hydrology. *Icarus* 198: 37-56.

Fassett, C., S. Kadish, J. Head, S. Solomon, and R. Strom. 2011. The global population of large craters on Mercury and comparison with the Moon. *Geophysical Research Letters* 38: 10202.

Feldman, W., W. Boynton, R. Tokar, T. Prettyman, O. Gasnault, S. Squyres, R. Elphic, D. Lawrence, S. Lawson, S. Maurice, G. McKinney, K. Moore, and R. Reedy. 2002. Global Distribution of Neutrons from Mars: Results from Mars Odyssey. *Science* 297: 75-78.

Forget, F., R. Haberle, F. Montmessin, B. Levrard, and J. Head. 2006. Formation of Glaciers on Mars by Atmospheric Precipitation at High Obliquity. *Science* 311: 368-371.

Forget, F., F. Hourdin, R. Fournier, C. Hourdin, O. Talagrand, M. Collins, S. Lewis, P. Read, and J-P. Huot. 1999. Improved general circulation models of the Martian atmosphere from the surface to above 80 km. *Journal of Geophysical Research* 104: 24155-24176.

Frigeri, A., T. Hare, M. Neteler, A. Coradini, C. Federico, and R. Orosei. 2011. A working environment for digital planetary data processing and mapping using ISIS and GRASS GIS. *Planetary and Space Science* 59 (11–12): 1265-1272.

Goodchild, M., L. Steyaert, B. Parks, and C. Johnston. (eds) 1996. *GIS and environmental modeling: progress and research issues*: John Wiley & Sons.

Haberle, R., J. Murphy, and J. Schaeffer. 2003. Orbital change experiments with a Mars general circulation model. *Icarus* 161 (1): 66-89.

Haberle, R., C. McKay, J. Schaeffer, N. Cabrol, E. Grin, A. Zent, and R. Quinn. 2001. On the possibility of liquid water on present-day Mars. *Journal of Geophysical Research* 106: 23317-23326.

Hare, T. 2014. USGS Planetary GIS Web Server - PIGWAD. http://webgis.wr.usgs.gov/ (accessed 6 March 2014).

Hare, T., J. Skinner, C. Fortezzo, K. Tanaka, and R. Nava. 2012. The Astrogeology Mapping, Remote-Sensing, Cartography, Technology, and Research (MRCTR) GIS Lab. Lunar and Planetary Science Conference 43: 2871.

Hayward, R., T. Titus, T. Michaels, A. Colaprete, C. Verba, and P. Christensen. 2009. Aeolian Dunes as Ground Truth for GCM and Mesoscale Modeling on Mars. Lunar and Planetary Science Conference 40: 2012.

Hayward, R., L. Fenton, T. Titus, A. Colaprete, and P. Christensen. 2012. Mars global digital dune database: MC-30. U.S. Geological Survey Open-File Report 2012–1259, pamphlet 8 p. and GIS data, scale 1:20,000,000.

Head, J., G. Neukum, R. Jaumann, H. Hiesinger, E. Hauber, M. Carr, P. Masson, B. Foing, H. Hoffmann, M. Kreslavsky, S. Werner, S. Milkovich, S. van Gasselt, and The HRSC Co-Investigator Team. 2005. Tropical to mid-latitude snow and ice accumulation, flow and glaciation on Mars. *Nature* 434: 346-351.

Head, J., C. Fassett, S. Kadish, D. Smith, M. Zuber, G. Neumann, and E. Mazarico. 2010. Global Distribution of Large Lunar Craters: Implications for Resurfacing and Impactor Populations. *Science* 329: 1504-1507.

Head, J., and D. Marchant. 2003. Cold-based mountain glaciers on Mars: Western Arsia Mons. *Geology* 31: 641-645.

Head, J., J. Mustard, M. Kreslavsky, R. Milliken, and D. Marchant. 2003. Recent ice ages on Mars. *Nature* 426: 797-802.

Hecht, M. 2002. Metastability of Liquid Water on Mars. *Icarus* 156: 373-386.

Heldmann, J., E. Carlsson, H. Johansson, M. Mellon, and O. Toon. 2007. Observations of martian gullies and constraints on potential formation mechanisms. *Icarus* 188: 324-344.

Heldmann, J., and M. Mellon. 2004. Observations of martian gullies and constraints on potential formation mechanisms. *Icarus* 168: 285-304.

Hynek, B., M. Beach, and M. Hoke. 2010. Updated global map of Martian valley networks and implications for climate and hydrologic processes. *Journal of Geophysical Research (Planets)* 115: 9008.

IPCC. 2007. *Contribution of Working Groups I, II and III to the Fourth Assessment Report of the Intergovernmental Panel on Climate Change*. Geneva, Switzerland, Cambridge University Press.

Kerber, L., J. Head, J-B. Madeleine, F. Forget, and L. Wilson. 2012. The dispersal of pyroclasts from ancient explosive volcanoes on Mars: Implications for the friable layered deposits. *Icarus* 219: 358-381.

Kneissl, T., D. Reiss, S. van Gasselt, and G. Neukum. 2010. Distribution and orientation of northern-hemisphere gullies on Mars from the evaluation of HRSC and MOC-NA data. *Earth and Planetary Science Letters* 294: 357-367.

Koziol, B. 2013. OpenClimateGIS: A Python Geoprocessing Framework for Climate Datasets. https://earthsystemcog.org/site_media/projects/openclimategis/Koziol_2013_FOSS4G.pdf (accessed 24 April 2014).

Kreslavsky, M., and J. Head. 1999. Kilometer-scale slopes on Mars and their correlation with geologic units: Initial results from Mars Orbiter Laser Altimeter (MOLA) data. *Journal of Geophysical Research* 104: 21911-21924.

Kreslavsky, M., and J. Head. 2000. Kilometer-scale roughness of Mars: Results from MOLA data analysis. *Journal of Geophysical Research* 105: 26695-26711.

Kreslavsky, M., and J. Head. 2002. Fate of outflow channel effluents in the northern lowlands of Mars: The Vastitas Borealis Formation as a sublimation residue from frozen ponded bodies of water. *Journal of Geophysical Research* 107: 5121.

Laskar, J., A. Correia, M. Gastineau, F. Joutel, B. Levrard, and P. Robutel. 2004. Long term evolution and chaotic diffusion of the insolation quantities of Mars. *Icarus* 170: 343-364.

Laskar, J., B. Levrard, and J. Mustard. 2002. Orbital forcing of the martian polar layered deposits. *Nature* 419: 375-377.

Levy, J., J. Head, D. Marchant, J. Dickson, and G. Morgan. 2009. Geologically recent gully-polygon relationships on Mars: Insights from the Antarctic Dry Valleys on the roles of permafrost, microclimates, and water sources for surface flow. *Icarus* 201: 113-126.

Lucchitta, B. 1981. Mars and Earth - Comparison of cold-climate features. *Icarus* 45: 264-303.

Madeleine, J-B., F. Forget, J. Head, B. Levrard, F. Montmessin, and E. Millour. 2009. Amazonian northern mid-latitude glaciation on Mars: A proposed climate scenario. *Icarus* 203: 390-405.

Madeleine, J-B., J. Head, F. Forget, T. Navarro, E. Millour, A. Spiga, A. Colaitis, F. Montmessin, and A. Määttänen. 2013. What Defines a Martian Glacial State? Analysis of the Mars Climate System Under Past Conditions Using the new LMD Global Climate Model. Lunar and Planetary Science Conference 44: 1895.

Malin, M. 2010. Mars Reconnaissance Orbiter (MRO) Context Camera (CTX). http://www.msss.com/all_projects/mro-ctx.php (accessed 7 March 2014).

Malin, M., K. Edgett, L. Posiolova, S. McColley, and E. Noe-Dobrea. 2006. Present-Day Impact Cratering Rate and Contemporary Gully Activity on Mars. *Science* 314 (5805): 1573-1577.

Malin, M., J. Bell, B. Cantor, M. Caplinger, W. Calvin, R. Clancy, K. Edgett, L. Edwards, R. Haberle, P. James, S. Lee, M. Ravine, P. Thomas, and M. Wolff. 2007. Context Camera Investigation on board the Mars Reconnaissance Orbiter. *Journal of Geophysical Research (Planets)* 112, doi: 10.1029/2006JE002808.

Malin, M., and K. Edgett. 2000. Evidence for Recent Groundwater Seepage and Surface Runoff on Mars. *Science* 288: 2330-2335.

Malin, M., and K. Edgett. 2001. Mars Global Surveyor Mars Orbiter Camera: Interplanetary cruise through primary mission. *Journal of Geophysical Research* 106: 23429-23570.

Matplotlib Basemap Toolkit 2014. Welcome to the Matplotlib Basemap Toolkit documentation. http://matplotlib.org/basemap/ (accessed 23 June 2014).

McCleese, D., J. Schofield, F. Taylor, S. Calcutt, M. Foote, D. Kass, C. Leovy, D. Paige, P. Read, and R. Zurek. 2007. Mars Climate Sounder: An investigation of thermal and water vapor structure, dust and condensate distributions in the atmosphere, and energy balance of the polar regions. *Journal of Geophysical Research (Planets)* 112: doi: 10.1029/2006JE002790.

McEwen, A., M. Banks, N. Baugh, K. Becker, A. Boyd, J. Bergstrom, R. Beyer, E. Bortolini, N. Bridges, S. Byrne, B. Castalia, F. Chuang, L. Crumpler, I. Daubar, A. Davatzes, D. Deardorff, A. Dejong, W. Delamere, E. Noe Dobrea, C. Dundas, E. Eliason, Y. Espinoza, A. Fennema, K. Fishbaugh, T. Forrester, P. Geissler, J. Grant, J. Griffes, J. Grotzinger, V. Gulick, C. Hansen, K. Herkenhoff, R. Heyd, W. Jaeger, D. Jones, B. Kanefsky, L. Keszthelyi, R. King, R. Kirk, K. Kolb, J. Lasco, A. Lefort, R. Leis, K. Lewis, S. Martinez-Alonso, S. Mattson, G. McArthur, M. Mellon, J. Metz, M. Milazzo, R. Milliken, T. Motazedian, C. Okubo, A. Ortiz, A. Philippoff, J. Plassmann, A. Polit, P. Russell, C. Schaller, M. Searls, T. Spriggs, S. Squyres, S. Tarr, N. Thomas, B. Thomson, L. Tornabene, C. van Houten, C. Verba, C. Weitz, and J. Wray. 2010. The High Resolution Imaging Science Experiment (HiRISE) during MRO's Primary Science Phase (PSP). *Icarus* 205: 2-37.

Milliken, R., J. Mustard, and D. Goldsby. 2003. Viscous flow features on the surface of Mars: Observations from high-resolution Mars Orbiter Camera (MOC) images. *Journal of Geophysical Research (Planets)* 108: 5057.

Mischna, M., M. Richardson, R. Wilson, and D. McCleese. 2003. On the orbital forcing of Martian water and CO2 cycles: A general circulation model study with simplified volatile schemes. *Journal of Geophysical Research (Planets)* 108: 5062.

MRCTR. 2014. Mars Crater Catalog by Stuart Robbins. http://astrogeology.usgs.gov/search/details/Mars/Research/Craters/RobbinsCrater Database_20120821/zip (accessed 21 April 2014).

Mustard, J., C. Cooper, and M. Rifkin. 2001. Evidence for recent climate change on Mars from the identification of youthful near-surface ground ice. *Nature* 412: 411-414.

Neukum, G., R. Greeley, H. Hiesinger, and P. Pinet. 2010. Mars geology from three - dimensional mapping by the High Resolution Stereo Camera (HRSC) Experiment on Mars Express. An introduction to the special issue of Earth Planetary Science Letters. *Earth and Planetary Science Letters* 294: 183-184.

Nier, A., W. Hanson, A. Seiff, M. McElroy, N. Spencer, R. Duckett, T. Knight, and W. Cook. 1976. Composition and structure of the Martian atmosphere: Preliminary results from Viking 1. *Science* 193 (4255): 786-788.

Noman, N., D. Zimble, and K. Sigwart. 2013. Using netCDF and HDF in ArcGIS. Federal GIS Conference, Washington, D.C.

Phillips, R., B. Davis, K. Tanaka, S. Byrne, M. Mellon, N. Putzig, R. Haberle, M. Kahre, B. Campbell, L. Carter, I. Smith, J. Holt, S. Smrekar, D. Nunes, J. Plaut, A. Egan, T. Titus, and R. Seu. 2011. Massive CO_2 Ice Deposits Sequestered in the South Polar Layered Deposits of Mars. *Science* 332: 838-841.

Pierce, T., and D. Crown. 2003. Morphologic and topographic analyses of debris aprons in the eastern Hellas region, Mars. *Icarus* 163: 46-65.

Reiss, D., G. Erkeling, K. Bauch, and H. Hiesinger. 2010. Evidence for present day gully activity on the Russell crater dune field, Mars. *Geophysical Research Letters* 37 (6): doi: 10.1029/2009GL042192.

Reiss, D., S. van Gasselt, G. Neukum, and R. Jaumann. 2004. Absolute dune ages and implications for the time of formation of gullies in Nirgal Vallis, Mars. *Journal of Geophysical Research (Planets)* 109: 06007.

Rew, R., and G. Davis. 1990. NetCDF: an interface for scientific data access. *Computer Graphics and Applications, IEEE* 10 (4): 76-82.

Robbins, S., and B. Hynek. 2012. A new global database of Mars impact craters ≥1 km: 1. Database creation, properties, and parameters. *Journal of Geophysical Research (Planets)* 117: 5004.

Satoh, M. 2013. *Atmospheric circulation dynamics and general circulation models*: UK: Springer Science & Business.

Schon, S., J. Head, and C. Fassett. 2009. Unique chronostratigraphic marker in depositional fan stratigraphy on Mars: Evidence for ~1.25 Ma old gully activity and surficial meltwater origin. *Geology* 37: 207-210.

Shean, D., J. Head, J. Fastook, and D. Marchant. 2007. Recent glaciation at high elevations on Arsia Mons, Mars: Implications for the formation and evolution of large tropical mountain glaciers. *Journal of Geophysical Research (Planets)* 112: 03004.

Shean, D., J. Head, and D. Marchant. 2005. Origin and evolution of a cold-based tropical mountain glacier on Mars: The Pavonis Mons fan-shaped deposit. *Journal of Geophysical Research (Planets)* 110: 05001.

Smith, P., L. Tamppari, R. Arvidson, D. Bass, D. Blaney, W. Boynton, A. Carswell, D. Catling, B. Clark, T. Duck, E. DeJong, D. Fisher, W. Goetz, Haraldur P. Gunnlauggson, M. Hecht, V. Hipkin, J. Hoffman, S. Hviid, H. Keller, S. Kounaves, C. Lange, M. Lemmon, M. Madsen, W. Markiewicz, J. Marshall, C. McKay, M. Mellon, D. Ming, R. Morris, W. Pike, N. Renno, U. Staufer, C. Stoker, P. Taylor, J. Whiteway, and A. Zent. 2009. H_2O at the Phoenix Landing Site. *Science* 325: 58-61.

Squyres, S., J. Grotzinger, R. Arvidson, J. Bell, W. Calvin, P. Christensen, B. Clark, J. Crisp, W. Farrand, K. Herkenhoff, J. Johnson, G. Klingelhöfer, A. Knoll, S. McLennan, H. McSween, R. Morris, J. Rice, R. Rieder, and L. Soderblom. 2004. In Situ Evidence for an Ancient Aqueous Environment at Meridiani Planum, Mars. *Science* 306: 1709-1714.

Steyaert, L., and M. Goodchild. 1994. Integrating GIS and environmental simulation modeling. In *Environmental Information Management and Analysis: Ecosystem to Global Scales*, ed. W. Michener, J. Brunt and S. Stafford, 333-356. UK: Taylor & Francis.

Streit, U., and K. Wiesmann. 1996. Problems of integrating GIS and hydrological models. In *Spatial analytical perspectives on GIS,* ed. M. Fischer, H. Scholten, and D. Unwin, D., 161-174. UK: Taylor & Francis.

Telis, P. 2007. A Quick Guide to Using EDEN NetCDF Files in ArcGIS 9.2. Everglades Depth Estimation Network.

http://sofia.usgs.gov/eden/edenapps/Quick_Guide_Using_EDEN_NetCDF_Fil es_ArcGIS.pdf (accessed 5 March 2014).

Vincendon, M., J. Mustard, F. Forget, M. Kreslavsky, A. Spiga, S. Murchie, and J-P. Bibring. 2010. Near-tropical subsurface ice on Mars. *Geophysical Research Letters* 37: 01202.

Whiteaker, T. 2006. Animating NetCDF Data in ArcMap. http://www.crwr.utexas.edu/gis/gishydro06/SpaceAndTime/NetCDF/Anim ating netCDF Data in ArcMap.htm. (accessed 5 March 2014).

Wilson, R., and K. Hamilton. 1996. Comprehensive model simulation of thermal tides in the Martian atmosphere. *Journal of Atmospheric Sciences* 53: 1290-1326.

Xiaolong, H. 2012. Construction and Application of Soil Moisture Data Model Used NetCDF Format Based on GIS. *Geospatial Information* 5: 024.

Xiong, C., and L. Wang. 2010. Study of Image Display with NetCDF Data on WebGIS. Second International Conference on Information Technology and Computer Science (ITCS).

Zuber, M., S. Solomon, R. Phillips, D. Smith, G. Tyler, O. Aharonson, G. Balmino, W. Banerdt, J. Head, C. Johnson, F. Lemoine, P. McGovern, G. Neumann, D. Rowlands and S. Zhong. 2000. Internal Structure and Early Thermal Evolution of Mars from Mars Global Surveyor Topography and Gravity. *Science* 287: 1788-1793.

APPENDIX A: Script for generating animation loops

The following is the Python script used to construct animations of temperature and

pressure conditions using GCM simulations. The geodatabase of gullies is incorporated

as a layer in the template mxd file (mxdpath).

This script is accessible via GitHub at the following address:

https://github.com/jaydickson/GCM-GIS_Integration/blob/master/jaydickson_GCM-GIS-

Integration_visualization.py

- - -

```
##This script generates a map for each timestep in a 5352 band GCM simulation
##Input obliquity to choose which simulation to run; default temp/pressure values are set
        to the triple point of water
##Jay Dickson - Brown U./USC - May, 2014
##jdickson@brown.edu

import os
import arcpy
from arcpy import env
from arcpy.sa import *

arcpy.CheckOutExtension("Spatial")

##Set local variables
obliquity = 35
scratchspace = "C:/Users/jdickson/Documents/Projects/Mars/GCM-Geodatabase-
        Integration/" + str(obliquity) + "deg/"
workspace = "C:/Users/jdickson/Documents/Projects/Mars/GCM-Geodatabase-
        Integration/GlobalGullyDatabase.gdb/"
slloc="C:/Users/jdickson/Documents/Projects/Mars/GCM-Geodatabase-
        Integration/MarsPressureStretch612-1200.lyr"
flloc="C:/Users/jdickson/Documents/Projects/Mars/GCM-Geodatabase-
        Integration/MarsTempContour273-293.lyr"
mxdPath = "C:/Users/jdickson/Documents/Projects/Mars/GCM-Geodatabase-
        Integration/GCMBasemap.mxd"

count = 1
```

```python
##Generate map for each band within GCM simulation
while (count < 5353):
    ##Set in-loop variables
    count_string = "0000" + str(count)
    count_label = count_string[-5:]
    inRasterPressure = workspace + "obl" + str(obliquity) + "_pSurf_MarsEC/Band_" +
        str(count)
    inRasterTemp = workspace + "obl" + str(obliquity) + "_tSurf_MarsEC/Band_" +
        str(count)

    ##Create pressure raster nulled below 6.11 mb (611.73 pascals)
    print "Extracting: Band" + count_label
    arcpy.CopyRaster_management(inRasterPressure, scratchspace + "Band" +
        count_label + ".tif","#","#","#","NONE","NONE","#")
    print "Nulling all negative values: Band" + count_label
    arcpy.Resample_management(scratchspace + "Band" + count_label +
        ".tif",scratchspace + "Band" + count_label + "_resample.tif","22227.965994
        22227.965994","CUBIC")
    outSetNull = SetNull(scratchspace + "Band" + count_label +
        "_resample.tif",scratchspace + "Band" + count_label + "_resample.tif", "VALUE
        < 611.73")
    outSetNull.save(scratchspace + "Band" + count_label + "_nulled.tif")

    ##Create temperature contour map nulled below 273 K
    arcpy.CopyRaster_management(inRasterTemp, scratchspace + "Temp_Band" +
        count_label + ".tif","#","#","#","NONE","NONE","#")
    print "Nulling all negative values: Band" + count_label
    arcpy.Resample_management(scratchspace + "Temp_Band" + count_label +
        ".tif",scratchspace + "Temp_Band" + count_label +
        "_resample.tif","22227.965994 22227.965994","CUBIC")
    arcpy.gp.Con_sa(scratchspace + "Temp_Band" + count_label +
        "_resample.tif",scratchspace + "Temp_Band" + count_label +
        "_resample.tif",scratchspace + "Temp_Band" + count_label +
        "_nulled.tif","#","""""VALUE" > 272""")
    arcpy.gp.Contour_sa(scratchspace + "Temp_Band" + count_label +
        "_nulled.tif",scratchspace + "Temp_Band" + count_label +
        "_ctr_05.shp","5","273","1")

    ##Delete temporary rasters
    arcpy.Delete_management(scratchspace + "Band" + count_label + ".tif")
    arcpy.Delete_management(scratchspace + "Band" + count_label + "_resample.tif")
    arcpy.Delete_management(scratchspace + "Temp_Band" + count_label + ".tif")
    arcpy.Delete_management(scratchspace + "Temp_Band" + count_label +
        "_resample.tif")
    arcpy.Delete_management(scratchspace + "Temp_Band" + count_label + "_nulled.tif")
```

```python
##Set variables for generating map
rasterPath = scratchspace + "Band" + count_label + "_nulled.tif"
featurePath = scratchspace + "Temp_Band" + count_label + "_ctr_05.shp"
featureLayerName = "ftemp" + count_label
rasterLayerName = "temp"

##Add pressure raster to map, set symbology to slloc, blend at 70% opacity
md = arcpy.mapping.MapDocument(mxdPath)
df = arcpy.mapping.ListDataFrames(md)[0]
result = arcpy.MakeRasterLayer_management(rasterPath, rasterLayerName)
layer = result.getOutput(0)
arcpy.mapping.AddLayer(df, layer, 'TOP')

sl=arcpy.mapping.Layer(slloc)
nl=arcpy.mapping.ListLayers(md)[0]
arcpy.mapping.UpdateLayer(df,nl,sl,"True")
nl.transparency = 70

##Add temperature contour to map, set symbology to flloc
featureresult = arcpy.MakeFeatureLayer_management(featurePath, featureLayerName)
featurelayer = featureresult.getOutput(0)
arcpy.mapping.AddLayer(df, featurelayer, 'TOP')

fl=arcpy.mapping.Layer(flloc)
al=arcpy.mapping.ListLayers(md)[0]
arcpy.mapping.UpdateLayer(df,al,fl,"True")

##Export map
arcpy.mapping.ExportToJPEG(md, "Z:/Desktop/" + str(obliquity) + "/Band_" +
    count_label + ".jpg",resolution = 150)

##Delete pressure raster and temperature contour feature class
arcpy.Delete_management(rasterPath)
arcpy.Delete_management(featurePath)

print "Completed Band " + count_label
count = count + 1

print "Process completed"
```

APPENDIX B: Script for extracting GCM values from Geodatabase

The following is the Python code used to extract temperature/pressure conditions from

gully locations.

This script is accessible via GitHub at the following address:

https://github.com/jaydickson/GCM-GIS_Integration/blob/master/jaydickson_GCM-GIS-

Integration_extraction.py

- - -


```python
##This script extracts the number of timesteps at each GCM cell when conditions surpass
        the triple point of water
##Input obliquity to choose which simulation to use
##Jay Dickson - Brown U./USC - May 2014
##jdickson@brown.edu

import os
import arcpy
from arcpy import env
from arcpy.sa import *

arcpy.CheckOutExtension("Spatial")

##Set local variables
obliquity = 35
scratchspace = "C:/Users/jdickson/Documents/Projects/Mars/GCM-Geodatabase-
        Integration/"
workspace = "C:/Users/jdickson/Documents/Projects/Mars/GCM-Geodatabase-
        Integration/GlobalGullyGeodatabase.gdb/"
JobName = "AllGullies" + str(obliquity)
fc = workspace + "MarsGullies/PixelsWithGullies"
TempLayer = scratchspace + "temp_temp.shp"
PressLayer = scratchspace + "press_temp.shp"
prj = "C:/Users/Public/Documents/Mars_GIS/MarsEC0.prj"
cursor = arcpy.SearchCursor(fc)

##Create folder to store tempeorary data
arcpy.CreateFolder_management(scratchspace, JobName)
```

```python
##Extract all temperature and pressure values from all points; iterate through bands in
        GCM simulation
count = 1

print "Extracting Temperature and Pressure values..."

while (count < 5353):

    print "Extracting: " + str(count)

    ##Extract values
    arcpy.gp.ExtractValuesToPoints_sa(fc,workspace + "obl" + str(obliquity) +
        "_tSurf_MarsEC/Band_" + str(count),TempLayer)
    arcpy.gp.ExtractValuesToPoints_sa(fc,workspace + "obl" + str(obliquity) +
        "_pSurf_MarsEC/Band_" + str(count),PressLayer)

    ##Add field to temporary temperature feature class, set values to extracted temperature
        values
    arcpy.AddField_management(TempLayer, "TempK", "DOUBLE")
    arcpy.CalculateField_management(TempLayer, "TempK", "!RASTERVALU!",
        "PYTHON_9.3")
    arcpy.DeleteField_management(TempLayer, "RASTERVALU")

    ##Add field to temporary pressure feature class, set values to extracted pressure values
    arcpy.AddField_management(PressLayer, "Pressure", "DOUBLE")
    arcpy.CalculateField_management(PressLayer, "Pressure", "!RASTERVALU!",
        "PYTHON_9.3")
    arcpy.DeleteField_management(PressLayer, "RASTERVALU")

    ##Join temperature & pressure features by OBJECTID
    arcpy.JoinField_management(TempLayer, "OBJECTID", PressLayer,
        "OBJECTID","Pressure")

    ##Make joined feature class permanent; delete temporary feature classes
    arcpy.CopyFeatures_management(TempLayer,scratchspace + JobName + "/" +
        JobName + "_" + str(count) + ".shp")
    count = count + 1

arcpy.Delete_management(TempLayer)
arcpy.Delete_management(PressLayer)

##Set more local variables
arcpy.env.workspace = scratchspace + JobName + "/"
featureclasses = arcpy.ListFeatureClasses()
```

```
##Set count to last functional value from above; needed for importing spatial reference of
      subsequent feature class
count = count - 1

##Create feature class that will compile features that surpass triple point; set conditional
      statement
arcpy.CreateFeatureclass_management(scratchspace + JobName, JobName + "_all.shp",
      "POINT", scratchspace + "/" + JobName + "/" + JobName + "_" + str(count) +
      ".shp", "DISABLED", "DISABLED", prj)
whereClause = "TempK > 273.16 and Pressure > 611.73"

##Iterate through all feature classes and extract all locations that surpass triple point;
      append those to new feature class
count = 1

print "Extracting water locations..."
for feature in featureclasses:
    print "Extracting: " + str(count)
    arcpy.MakeFeatureLayer_management(feature, "temp_lyr" + str(count), whereClause)
    arcpy.Append_management("temp_lyr" + str(count), scratchspace + JobName + "/" +
        JobName + "_all.shp")
    count = count + 1

##Create final feature class that includes the OBJECTID and N (total instances for each
      feature)
arcpy.CreateFeatureclass_management(scratchspace + JobName, JobName +
      "_count.shp", "POINT", "#", "DISABLED", "DISABLED", prj)
arcpy.AddField_management(JobName + "_count.shp","OBJECTID","TEXT")
arcpy.AddField_management(JobName + "_count.shp","N","TEXT")

##Count instances for each separate feature by OBJECTID; insert new row with
      OBJECTID and N
print "Counting instances at each point..."
count = 1

while count < 446:
    print "Counting: " + str(count)
    arcpy.MakeFeatureLayer_management(scratchspace + JobName + "/" + JobName +
        "_all.shp", "temp" + str(count), "\"OBJECTID\"=" + str(count))
    n = arcpy.GetCount_management("temp" + str(count))
    arcpy.Delete_management("temp" + str(count))
    cursor = arcpy.da.InsertCursor(JobName + "_count.shp",("OBJECTID","N"))
    cursor.insertRow((str(count), str(n)))
    count = count + 1

##Prepare final feature class with properly assigned fields
```

```python
finalshape = workspace + "MeltNumberCounts/" + JobName

##Join count data with original point using "ET_ID" and "FID" (subsequent iterations of
        OBJECTID)
arcpy.CopyFeatures_management(fc, finalshape)
arcpy.JoinField_management(finalshape,"ET_ID",scratchspace + JobName + "/" +
        JobName + "_count.shp","FID","N")
arcpy.Delete_management(scratchspace + JobName + "/" + JobName + "_all.shp")
arcpy.Delete_management(scratchspace + JobName + "/" + JobName + "_count.shp")

##Convert field "N" from TEXT to SHORT
arcpy.AddField_management(finalshape, "MeltNumber", "SHORT")
arcpy.CalculateField_management(finalshape, "MeltNumber", "!N!", "PYTHON_9.3")
arcpy.DeleteField_management(finalshape, "N")

print "Process Completed"
```

APPENDIX C: GCM Animation videos

Three movies were constructed and submitted as part of this project. These can be

viewed on the Spatial Sciences Institute website (http://spatial.usc.edu) and the following

captions describe their contents.

- - -

1. Video-01_25-obliquity.avi. Surface pressure (millibars) and surface temperature

(Kelvin) over the course of one Mars year at 25° obliquity and average pressure of

6 mb, which represents present-day conditions, with all gullies mapped in the

southern hemisphere in black. Pressure is represented by the color raster, with all

values below the triple point of water (6.11 mb) represented as null values.

Temperature is represented in 5 K contours, with all values below the triple point

of water (273 K) represented as null values. Animation spans one Mars year

starting at the beginning of northern hemisphere spring, and each frame represents

1/8 of a sol (a martian day, 24h 39m). Under these conditions, the majority of

gully sites occur in locations that are below the triple point of water for the entire

year.

2. Video-02_30-obliquity.avi. Surface pressure (millibars) and temperature (Kelvin) over

the course of one Mars year at 30° obliquity and average pressure of 8 mb, which

represents conditions ~380,000 years ago, with all gullies mapped in the southern

hemisphere in black. Pressure is represented by the color raster, with all values

below the triple point of water (6.11 mb) represented as null values. Temperature

is represented in 5 K contours, with all values below the triple point of water (273

80

K) represented as null values. Animation spans one Mars year starting at the beginning of the northern hemisphere spring, and each frame represents 1/8 of a sol (a martian day, 24h 39m). During the southern summer (last quarter of video) Mars' closer proximity to the sun sublimates more ice from the polar caps, increasing pressure such that most gullies do experience conditions above the triple point of water. However, gullies at higher elevations do not meet these conditions.

3. Video-03_35-obliquity.avi. Surface pressure (millibars) and surface temperature (Kelvin) over the course of one Mars year at 35° obliquity and average pressure of 10 mb, which represents conditions ~625,000 years ago, with all gullies mapped in the southern hemisphere in black. Pressure is represented by the color raster, with all values below the triple point of water (6.11 mb) represented as null values. Temperature is represented in 5 K contours, with all values below the triple point of water (273 K) represented as null values. Animation spans one Mars year starting at the beginning of northern hemisphere spring, and each frame represents 1/8 of a sol (a martian day, 24h 39m). In this simulation, surface pressure at nearly all locations on Mars for the entire year surpass the triple point, such that all gullies could potentially form by the melting of surface/near-surface ice deposits.